*Work supported by National Science Foundation, under Grant No. GP 7257.

†Present address: Institut d'Astrophysique, Université de Liège, Cointe-Sclessin, Belgium.

[1]H. Primakoff and T. Holstein, Phys. Rev. 55, 218 (1938).

[2]B. M. Axilrod and E. Teller, J. Chem. Phys. 11, 299 (1943).

[3]These retardation effects can be understood as follows: The root-mean-square electric (and magnetic) field, due to the vacuum fluctuations of the electromagnetic field, induces a dipole moment in the atoms, which dipoles then interact. For two atoms separated by a distance R, only those fluctuations with $\lambda \gtrsim R$ will be effective.

[4]L. Jansen, in *Advances in Quantum Chemistry*, edited by P.-O. Löwdin (Academic, New York, 1965) Vol. 2.

[5]R. P. Feynman, Phys. Rev. 80, 440 (1950).

[6]R. P. Feynman, Rev. Mod. Phys. 20, 367 (1948).

[7]R. P. Feynman, Phys. Rev. 84, 108 (1951).

[8]Actually, expression (6) is ill defined because it contains infrared divergences [any transition must involve the emission of an (infinite) number of soft photons]!

[9]These techniques have been used in the polaron problems by T. D. Schultz, in *Polarons and Excitons*, edited by C. G. Kuper and G. D. Whitfield (Plenum, New York, 1963); and H. Haken, *ibid.*

[10]F. Bloch and A. Nordsieck, Phys. Rev. 52, 54 (1937).

[11]Here, of course we are making an adiabatic assumption that ϵ is a positive infinitesimal quantity; we shall be interested in the $\lim \epsilon \to 0^+$.

[12]In the case that $[A, [A, B]] = [B, [A, B]] = 0$, we have $e^{A+B} = e^A e^B e^{-[A,B]/2}$.

PHYSICAL REVIEW A VOLUME 1, NUMBER 5 MAY 1970

Theory of a High-Intensity Gas Laser*

B. J. Feldman and M. S. Feld
Department of Physics, Massachusetts Institute of Technology, Cambridge, Massachusetts 02139

(Received 25 August 1969)

This paper presents a semiclassical theory of a single-mode gas laser valid for essentially arbitrary values of field intensity. The theory is formulated in terms of an ensemble-averaged form of the density-matrix equations of motion involving a single set of coordinates. The polarization and the population-inversion density are expanded in spatial Fourier components. One obtains a set of coupled difference equations in the Fourier coefficients y_n, which may be solved subject to appropriate boundary conditions on y_n for large n. The solutions may be expressed in terms of continued fractions in the general case, and in closed form in important special cases. Quantities of interest are evaluated by computer. The steady-state laser intensity and frequency are obtained from the coupled electromagnetic field equations as functions of the cavity parameters and the linear gain of the amplifying medium. At moderate values of field intensity, the velocity distribution of the space-averaged population inversion density exhibits a fine structure for low-velocity atoms superimposed on the usual broader depletion. This structure is a manifestation of the coherent ringing of the amplifying medium. The results are compared with those obtained in the rate-equation approximation, and with the recent work of Stenholm and Lamb. Discrepancies with the latter paper are explained.

1. INTRODUCTION

Our understanding of the dynamics of a gas laser begins with the theory of Lamb[1,2] which, in an elegant formalism, brought together the quantum-mechanical, statistical-mechanical, and electromagnetic aspects of the problem. The original treatment was limited to weak-field saturation (third-order polarization). More recently, Stenholm and Lamb[3] have extended the formalism to the case of a single-mode laser of arbitrary field intensity. This case is of particular interest because of a recently introduced technique[4] for inducing high-power single moding in gas lasers.

The present paper approaches the single-mode laser problem from a point of view[5,6] which considerably simplifies the calculation by dealing directly with the equations of motion describing an entire atomic velocity ensemble in terms of a single set of coordinates. This approach is mathematically equivalent to that of Ref. 3. Nevertheless, our results differ in some important respects.

Because of the coherent nature of the atom-field interaction, it is important to include coherent population effects (pulsations in the inversion density) in formulating gas-laser problems.[7] In the past, theories including such effects have generally been formulated in one of two ways. Several authors[1, 2, 8] have adopted the procedure of first computing the response of a single atom at coordinates $\{z, t\}$ moving with velocity v produced at coordinates $\{z_0, t_0\}$, and then explicitly summing over all possible initial conditions. In another approach,[3, 9, 10] the state of an ensemble-averaged system moving with velocity v at coordinates $\{z, t\}$ is obtained by solving a set of equations which relates this state to another state at coordinates $\{\hat{z}, \hat{t}\}$. Both of these approaches require solving a set of integral or integrodifferential equations. In our approach, the differential equations of motion can be solved directly.

The ensemble-averaged equations of motion are derived in Sec. 2. In Sec. 3 these equations are immediately solved to obtain a system of coupled difference equations equivalent to those of Stenholm and Lamb. In Sec. 4, the coupled equations are combined with the electromagnetic field equations to obtain expressions for the steady-state laser intensity and frequency. Inspection of the coupled difference equations in Sec. 5 reveals two types of solutions, one which diverges under various conditions. It is shown that the other type, which has good convergence properties, is the physically acceptable one. Solutions to the coupled difference equations are obtained in Sec. 6. In general, solutions may be expressed in terms of continued fractions.[3] However, in important special cases analytical expressions are obtained. The results are presented in Sec. 7. We find that spatial variations of high harmonic content in the polarization and in the population inversion density vanish, in contrast with the findings of Ref. 3. These discrepancies are explained. Examination of the velocity distribution of the inversion density using both analytical expressions and continued fractions reveals that with increasing field strength an additional feature not predicted in perturbation treatments[2, 11] nor in rate-equation treatments,[7] manifests itself when the laser is tuned to the center of the atomic-gain profile. This feature consists of fine structure in the population inversion density for low-velocity atoms, superposed upon the usual broader depletion. However, it is found that the central tuning dip (Lamb-dip) does not qualitatively differ in structure from predictions based on the rate equations. These results agree with those of Stenholm and Lamb.[3] The fine structure of the inversion density is interpreted in the frequency domain in terms of parametric processes, and in the time domain as a manifestation of coherent ringing of the amplifying medium.

2. ENSEMBLE-AVERAGED EQUATIONS OF MOTION

In this section we obtain an ensemble-averaged form of the density matrix equations of motion involving a single set of coordinates, which is applicable to gas-laser problems, i.e., problems involving resonant interaction of intense standing-wave fields with broad atomic velocity distributions. Our belief that one can deal directly with atomic velocity ensembles in this way has been motivated by the following considerations[5]: Imagine a Doppler-broadened atomic system with multiple levels interacting with intense monochromatic standing-wave fields. In the simple picture of atomic motion generally adopted, an atom produced at a particular position and time travels undeflected with constant axial velocity until its decay. Thus, one may deal separately with ensembles of atoms moving with different velocities. Let us focus our attention on one such group moving with axial velocity v. Note that by studying the response of this ensemble in a coordinate system also moving with velocity v, the problem reduces to one in which the atoms appear fixed; a situation for which it is well known[1, 12] that ensemble-averaged equations of motion may be derived. Thus, one can, in principle, calculate the rest-frame response of the atomic ensemble as a whole, then transform back into the laser rest frame. In the latter frame, the jth standing wave at frequency ν_j may be decomposed into a pair of travelling wave components at frequency ν_j of equal amplitude and opposite propagation directions. In the atomic rest frame, however, the field components appear Doppler shifted to frequencies

$$\nu_j^{\pm} = \nu \mp k_j v, \quad k_j = \nu_j / c \ , \tag{1}$$

the downshifted component propagating in the direction of atomic motion, the upshifted component propagating in the opposite direction. Thus, in the ensemble rest frame, the j-field standing-wave problem reduces to an ensemble of fixed atoms interacting with $2j$ travelling-wave fields. As a specific example, in the problem treated in this paper the single standing-wave field at frequency ν appears in the ensemble rest frame as two applied fields at frequencies $\nu \pm kv$. Because of the nonlinear nature of the interaction, these fields generate components of induced polarization not only at the fundamental frequencies $\nu \pm kv$, but also at sideband frequencies $\nu \pm 3kv$, $\nu \pm 5kv, \ldots$, as well as population fluctuations at frequencies $2kv$, $4kv, \ldots$. These sidebands react back and considerably influence the polarization at the fundamental frequencies.[13] Equivalently, one can view the problem in the laser rest frame, in which case the

sidebands manifest themselves as variations in *space*—polarization components at odd multiples of kz and population components at even multiples of kz—rather than variations in time.[13] We have found it more compact to treat the entire problem in the laser rest frame.[14] It is often easier, however, to envision the nonlinear interaction in the atomic rest frame, and we shall have occasion to refer to that picture later on.

A formal derivation is now given. Consider a Doppler-broadened multiple-level atomic system interacting with an electric field $\mathcal{E}(z,t)$ consisting of a number of intense monochromatic classical standing-wave components. Let us focus our attention on the evolution of a single atom moving with constant axial velocity component v produced[15] in level k at coordinates $\{z_o, t_o\}$, so that at a subsequent time t the atom will be found at position

$$z = z_o + v(t - t_o) \ . \tag{2}$$

The total Hamiltonian for the atom is

$$H(z,t) = H_0 + V(z,t), \tag{3}$$

where H_0 is the Hamiltonian of an isolated atom with stationary states ψ_j of energy $\hbar W_j$. The atom is coupled to the applied field by the interaction Hamiltonian

$$V(z,t) = -\mu\mathcal{E}(z,t) \ , \tag{4}$$

in which μ is the electric dipole operator. The atom's interaction with the applied field may be described by means of a density matrix with elements

$$\rho_{ij}(v,t;\ z_o,t_o,k) \ , \tag{5}$$

which obeys the familiar equation of motion

$$\frac{d}{dt}\rho(v,t;z_o,t_o,k) = -(i/\hbar)[H(z_o+v(t-t_o),t),\rho(v,t;z_o,t_o,k)] - \tfrac{1}{2}\{\Gamma,\rho(v,t;z_o,t_o,k)\} \ , \tag{6}$$

where the left-hand side is the total ("hydrodynamic") derivative of ρ, i.e., its total rate of change as one moves along with the atom. Here [ ] are commutator brackets and { } are anticommutator brackets, and H is the Hamiltonian matrix having elements

$$H_{ij} = \hbar W_j\delta_{ij} + V_{ij} \ , \tag{7}$$

$$\text{where } V_{ij} = -\mu_{ij}\mathcal{E}(z,t) \ , \tag{8}$$

with electric dipole matrix element

$$\mu_{ij} = \int_{\text{atom}} \psi_i^*\mu\psi_j\,dV \ . \tag{9}$$

In Eq. (6) relaxation has been introduced by means of the matrix Γ with elements

$$\Gamma_{ij} = \gamma_j\delta_{ij} \ , \tag{10}$$

where γ_j is the decay rate of level j. Note that in Eq. (6) an off-diagonal matrix element relaxes, in the absence of applied fields, at a rate

$$\gamma_{ij} = \tfrac{1}{2}(\gamma_i + \gamma_j) \tag{11}$$

as would be the case, for example, in radiative decay.[16] The expectation value of the induced dipole moment is

$$\text{Tr}[\mu\rho(v,t;z_o,t_o,k)] \ . \tag{12}$$

The net polarization, $P(v,z,t)dv$, due to atoms moving with velocity components in the interval between v and $v+dv$, is obtained by integrating this expression over initial coordinates and summing over levels of initial excitation. In the steady state, atoms in level k are produced at coordinates $\{z_o, t_o\}$, and with axial velocity components in the interval between v and $v+dv$ at a rate

$$n_k(v,z_o,t_o)\gamma_k dv \tag{13}$$

per unit volume, where $n_k(v,z_o,t_o)dv$, the background population density of level k in the interval between v and $v+dv$, may be assumed[17] to be independent of the applied field. Thus, making the approximation of evaluating n_k at $\{z,t\}$ instead of at $\{z_o,t_o\}$, $P(v,z,t)dv$ is given by

$$P(v,z,t)dv = \sum_k n_k\gamma_k dv\int_{-\infty}^{t} dt_o\int_{-\infty}^{\infty} dz_o\ \text{Tr}[\mu\rho(v,t;z_o,t_o,k)]\,\delta[z-z_o-v(t-t_o)] \ . \tag{14}$$

Introducing the ensemble-averaged density matrix

$$\rho(v,z,t) = \sum n_k\gamma_k\int_{-\infty}^{t} dt_o\int_{-\infty}^{\infty} dz_o\,\rho(v,t;z_o,t_o,k)\delta[z-z_o-v(t-t_o)] = \sum n_k\gamma_k\int_{-\infty}^{t} dt_o\,\rho[v,t;z-v(t-t_o),t_o,k] \ , \tag{15}$$

Eq. (14) may be written in the form

$$P(v,z,t)dv = \mathrm{Tr}[\mu\rho(v,z,t)]dv \ . \tag{16}$$

The total polarization due to atoms of all velocities is then given by

$$P(z,t) = \int_{-\infty}^{\infty} \mathrm{Tr}[\mu\rho(v,z,t)]dv \ . \tag{17}$$

To derive an equation of motion for $\rho(v,z,t)$ from that of $\rho'(v,t;z_o,t_o,k)$, consider the total derivative[18]

$$\frac{d}{dt}\rho(v,z,t) = v\left(\frac{\partial}{\partial z}+\frac{\partial}{\partial t}\right)\rho(v,z,t)$$
$$= \sum n_k\gamma_k \int_{-\infty}^{t} dt_o \ v\left(\frac{\partial}{\partial z}+\frac{\partial}{\partial t}\right)\rho[v,t;z-v(t-t_o),t_o,k] + \sum n_k\gamma_k\rho(v,t;z,t,k) \ . \tag{18}$$

The last term of the right-hand side is a boundary condition, namely, the value of ρ at $\{z,t\}$ for an atom produced at those same coordinates. According to our assumed initial conditions,[15] the elements of $\rho(v,t;z,t,k)$ obey the relationship

$$\rho_{ij}(v,t;z,t,k) = \delta_{ij}\delta_{jk} \ . \tag{19}$$

Defining a matrix ρ^0 describing the background population, with elements

$$\rho_{ij}{}^0 = n_i(v,z,t)\delta_{ij} \ , \tag{20}$$

we obtain

$$\frac{d}{dt}\rho(v,z,t) = \tfrac{1}{2}[\Gamma,\rho^0(v,z,t)\} + \sum n_k\gamma_k$$
$$\times \int_{-\infty}^{t} dt_o \frac{d}{dt}\rho[v,t;z-v(t-t_o),t_o,k] \ . \tag{21}$$

To transform Eq. (6) into an equation in $\rho(v,z,t)$, first multiply both sides by $\delta[z-z_o-v(t-t_o)]$ and sum up over z_o, t_o, and k. Performing the z_o integration, the L. H. side becomes

$$\sum n_k\gamma_k \int_{-\infty}^{t} dt_o \frac{d}{dt}\rho[v,t;z-v(t-t_o),t_o,k],$$

which is identical to the last term on the R. H. side of Eq. (21). In considering the R. H. side of Eq. (6), note that H becomes independent of z_o and t_o because of the δ function. We therefore obtain the ensemble-averaged equation of motion

$$\left(\frac{\partial}{\partial t}+v\frac{\partial}{\partial z}\right)\rho(v,z,t) = -\frac{i}{\hbar}[H(z,t),\rho(v,z,t)]$$
$$-\tfrac{1}{2}[\Gamma,\rho(v,z,t)-\rho^0(v,z,t)\}, \tag{22}$$

the desired result. A closely related derivation was given in Ref. 9, but with a different interpretation of the parametric dependences of ρ. Equation (22) may be obtained from Eq. (40) of Ref. 9 by equating $\hat{t}$ and t. It is perhaps worth reiterating that calculations are enormously simplified by dealing directly with Eq. (22) as interpreted above.

3. COUPLED EQUATIONS FOR A SINGLE-MODE LASER

We now apply the above results to the case of a single standing-wave field of arbitrary intensity interacting with a Doppler-broadened two-level atomic system, as would occur within a high-Q laser resonator of length L. In this case, the evolution of $\rho(v,z,t)$ is described by Eq. (22), with indices i,j,k referring to the upper and lower atomic energy levels, denoted by a and b, respectively (Fig. 1). The matrix elements of the interaction Hamiltonian [Eq. (8)] may now be written $V_{ab} = V_{ba} = \hbar V_o$, with

$$V_o(z,t) = -\frac{\mu_o}{\hbar}\mathcal{E}_o \sin kz \cos\nu t$$
$$= -(\mu_o\mathcal{E}_o/4i\hbar)[e^{i\nu t}(e^{ikz}-e^{-ikz}) - \mathrm{c.c.}] \ , \tag{23}$$

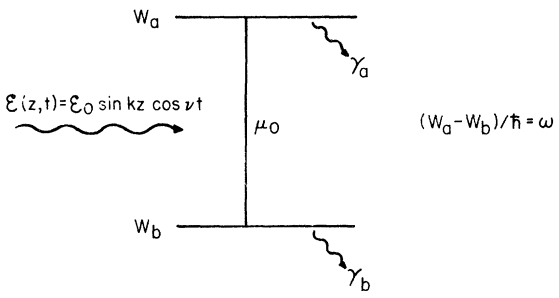

FIG. 1. Energy-level diagram for two-level atomic system, coupled to standing-wave field. Relaxation is introduced via decay rates γ_a and γ_b.

since $\mu_o = \mu_{ab}$ may be chosen to be real. The boundary condition imposed by the resonator is satisfied with

$$k = m\pi/L, \quad m = \text{a positive integer}. \tag{24}$$

From Eq. (16) the polarization of an ensemble of atoms with axial velocity components in the interval between v and $v+dv$ is

$$P(v,z,t)dv = \mu_o[\rho_{ab}(v,z,t) + \text{c.c.}]\,dv. \tag{25a}$$

The population inversion density in the interval dv, as influenced by the applied field, is given by

$$N(v,z,t)dv = [\rho_{aa}(v,z,t) - \rho_{bb}(v,z,t)]\,dv \ . \tag{25b}$$

Writing out Eq. (22) for the elements of $\rho(v,z,t)$, we have

$$\left(\frac{\partial}{\partial t} + v\frac{\partial}{\partial z} + i\omega\right)\rho_{ab} + \gamma_{ab}\rho_{ab} = iV_o(z,t)(\rho_{aa} - \rho_{bb}), \tag{26a}$$

$$\left(\frac{\partial}{\partial t} + v\frac{\partial}{\partial z}\right)\rho_{aa} + \gamma_a(\rho_{aa} - n_a) = iV_o(z,t)(\rho_{ab} - \rho_{ba}) \ , \tag{26b}$$

$$\left(\frac{\partial}{\partial t} + v\frac{\partial}{\partial z}\right)\rho_{bb} + \gamma_b(\rho_{bb} - n_b) = -iV_o(z,t)(\rho_{ab} - \rho_{ba}) \ , \tag{26c}$$

$$\text{and} \quad \rho_{ba} = \rho_{ab}^* \ , \tag{26d}$$

$$\text{where} \quad \omega = W_a - W_b > 0 \ . \tag{27}$$

These coupled equations may be solved by inserting V_o in complex form and inspecting the behavior of various possible time-varying components of ρ. The bracketed operators appearing on the left-hand sides of Eqs. (26) are of special significance in this regard because their eigenvalues eventually appear in the denominators of the expressions for the elements of ρ. The only important frequency components of ρ are those which lead to resonant denominators. Thus, the dominant frequency component of ρ_{ab} varies as $\exp(-i\nu t)$. Likewise, the only important contributions to ρ_{aa} and ρ_{bb} are time-independent. Therefore, a nearly complete solution of Eqs. (26) is of the form

$$\rho_{ab}(v,z,t) = e^{-i\nu t}\sum_{n=0}^{\infty}[\Pi_n^+(v)e^{inkz} + \Pi_n^-(v)e^{-inkz}] \ ; \tag{28a}$$

$$\text{likewise,} \quad \rho_{aa}(v,z,t) = \sum_{n=0}^{\infty}[a_n(v)e^{inkz} + \text{c.c.}] + n_a \ , \tag{28b}$$

$$\rho_{bb}(v,z,t) = \sum_{n=0}^{\infty}[b_n(v)e^{inkz} + \text{c.c.}] + n_b \ , \tag{28c}$$

since ρ_{aa} and ρ_{bb} are real. In writing these expressions the predominant spatial variations have been expressed as harmonics in kz. The possibility of additional slow z and t variations in n_a and n_b can be allowed for by considering $\Pi_n^{\pm}$, a_n and b_n to be slowly varying functions of these parameters.[19]

An important property of the solutions (28) follows from the iterative relationship between diagonal and off-diagonal elements of ρ: The (essentially) spatially constant portions of ρ_{aa} and ρ_{bb} couple nonlinearly through V_o to produce components of ρ_{ab} which vary at $\exp(\pm ikz)$; these react back on ρ_{aa} and ρ_{bb}, producing components at $\exp(\pm 2ikz)$, and so forth. It follows that in Eqs. (28) we may exclude all spatial harmonics in ρ_{ab} even in n, and in ρ_{aa} and ρ_{bb} odd in n. With this in mind, we proceed by substituting our trial solution, Eq. (28), into the coupled equations (26) and equating coefficients of like harmonics in z and t. The off-diagonal equations (26a) and (26b) lead to

$$\mathfrak{L}_{n'}^{+}\Pi_{n'}^{+} = \gamma_o s(d_{n'+1} - d_{n'-1}) \ , \tag{29a}$$

$$\mathfrak{L}_{n'}^{-}\Pi_{n'}^{-} = -\gamma_o s(d_{n'+1} - d_{n'-1})^* \ , \tag{29b}$$

$$\text{with} \quad n' = 1, 3, 5, \ldots \ . \tag{30}$$

(The notation is defined below.) The diagonal equations (26b) and (26c) lead to

$$d_0 = 2s[(\Pi_1^+ - \Pi_1^-) + \text{c.c.}] + N_o \ , \tag{31a}$$

$$\text{and} \quad M_{n''}d_{n''} = \gamma_o s[(\Pi_{n''+1}^+ - \Pi_{n''-1}^+) - (\Pi_{n''+1}^- - \Pi_{n''-1}^-)^*] \ , \tag{31b}$$

$$\text{with} \quad n'' = 2, 4, 6, \ldots \ . \tag{32}$$

In Eqs. (29) and (31), we have used the following notation:

$$d_{n''} = a_{n''} - b_{n''} \ , \tag{33a}$$

$$d_0=[(a_0-b_0)+\text{c.c.}]+N_o \quad , \tag{33b}$$

where $N_o(v,z,t)=n_a(v,z,t)-n_b(v,z,t)$, (34)

so that $N_0 dv$ is the (slowly varying) excitation density at coordinates $\{z,t\}$ in the interval between v and $v+dv$

$$\mathcal{L}_{n'}^{\pm}=\gamma_{ab}+i(\omega-\nu\pm n'kv) \quad , \tag{35}$$

$$\frac{1}{M_{n''}}=\frac{1}{\gamma_a+in''kv}+\frac{1}{\gamma_b+in''kv} \quad ; \tag{36}$$

and we have introduced the dimensionless parameter $\mathcal{S}$ as a measure of the degree of saturation:

$$\mathcal{S}=\mu_o\mathcal{E}_0/4\hbar\gamma_0 \quad , \tag{37}$$

with $\gamma_o=\gamma_a\gamma_b/\gamma_{ab}$. (38)

Equations (29) immediately imply that

$$\mathcal{L}_{n'}^{+}\Pi_{n'}^{+}=-(\mathcal{L}_{n'}^{-}\Pi_{n'}^{-})^*; \tag{39}$$

accordingly, Eq. (31b) becomes

$$M_{n''}d_{n''}=\gamma_o\mathcal{S}[(\mathcal{L}_{n''+1}^{+}/K_{n''+1})\Pi_{n''+1}^{+} - (\mathcal{L}_{n''-1}^{+}/K_{n''-1})\Pi_{n''-1}^{+}] \quad , \tag{40a}$$

and Eq. (31a) becomes

$$d_0=2\mathcal{S}[(\mathcal{L}_1^{+}/K_1)\Pi_1^{+}+\text{c.c.}]+N_0 \quad , \tag{40b}$$

with $$\frac{1}{K_{n'}}=\frac{1}{\mathcal{L}_{n'}^{+}}+\frac{1}{\mathcal{L}_{n'}^{-*}} \quad . \tag{41}$$

Equations (29a) and (40) constitute an infinite set of coupled difference equations. Since Π_n and d_n vanish for even and odd values of n, respectively, we may combine their equations into a more compact and symmetrical form. To this end we define

$$N_o y_{n'}=(\mathcal{L}_{n'}^{+}/K_{n'})\Pi_{n'}^{+} \quad , \quad n'=1,3,5,\ldots$$
$$R_{n'}=K_{n'} \quad , \qquad n'=1,3,5, \tag{42a}$$

$$N_o y_{n''}=d_{n''} \quad , \qquad n''=0,2,4,\ldots \quad .$$
$$R_{n''}=M_{n''} \quad , \qquad n''=0,2,4. \tag{42b}$$

Then Eqs. (29a) and (40) reduce to

$$R_n y_n=\gamma_o\mathcal{S}(y_{n+1}-y_{n-1}), \quad n=1,2,3,\ldots \quad , \tag{43a}$$

$$y_0=2\mathcal{S}(y_1+y_1^*)+1 \quad . \tag{43b}$$

An equivalent set of equations was first derived by Stenholm and Lamb[20] using more lengthy procedure.

4. CONNECTION WITH ELECTROMAGNETIC FIELD EQUATIONS

Once the y_n are determined, the physical parameters of the atomic system may be completely specified. For an ensemble characterized by parameters $\{v,z,t\}$ the polarization and population inversion density are readily available from Eqs. (25), (28), (33)–(35), (39), and (41)–(43):

$$P(v,z,t)=-\mu_o N_o\,\mathrm{Re}e^{i\nu t}\sum_{\text{odd } n}\left[\left(1+\frac{i(\omega-\nu)}{\gamma_{ab}+inkv}\right)\times y_n e^{inkz}-\left(1+\frac{i(\omega-\nu)}{\gamma_{ab}-inkv}\right)y_n^* e^{-inkz}\right], \tag{44}$$

$$N(v,z,t)=N_o[y_0+\sum_{\text{even } n>0}(y_n e^{inkz}+\text{c.c.})]. \tag{45}$$

We shall sometimes refer to the y_n's as the Fourier coefficients of N and P.[21] The net polarization $P(z,t)$ is obtained by summing Eq. (44) over all velocities [Eq. (17)]. The velocity dependence enters into $P(v,z,t)$ through the bracketed quantities in Eq. (44), the y_n's, and through N_0, the excitation density, which may be written in the form

$$N_o(v,z,t)=\bar{N}_o(z,t)W(v) \quad , \tag{46}$$

where $W(v)$ is the normalized atomic velocity distribution,

$$\int_{-\infty}^{\infty}W(v)\,dv=1 \quad . \tag{47}$$

In what follows we shall assume $\bar{N}_0$ to be independent of z and t. We can write

$$\mathcal{E}(z,t)=\mathrm{Re}(\mathcal{E}_o\sin kz\,e^{i\nu t}) \quad , \tag{48a}$$

$$P(z,t)=\mathrm{Re}\sum_{n\text{ odd}}(\chi_n^{+}\sin mkz + i\chi_n^{-}\cos nkz)\mathcal{E}_o e^{i\nu t} \quad , \tag{48b}$$

where $$\chi_n^{\pm}\mathcal{E}_o = -i\mu_o \bar{N}_o \int_{-\infty}^{\infty} W(v)\left[\pm\left(1+\frac{i(\omega-\nu)}{\gamma_{ab}+inkv}\right)\right.$$

$$\left.\times\, y_n + \left(1+\frac{i(\omega-\nu)}{\gamma_{ab}-inkv}\right)y_n^*\right]dv\ . \qquad (49)$$

The growth of the electromagnetic field within the laser cavity is related to the polarization induced in the sample through Maxwell's equations.[1,2] The resulting relationships may be written in the form

$$\frac{dU}{dt} = G - \frac{\nu}{Q}U\ , \qquad (50a)$$

$$\nu = \Omega/n_0\ . \qquad (50b)$$

Here U, the average energy density of the electromagnetic field, is given by

$$U = \frac{1}{L}\int_0^L \frac{\langle \mathcal{E}^2(z,t)\rangle}{4\pi}\,dz = \frac{\mathcal{E}_o^{\,2}}{16\pi}\ , \qquad (51)$$

where the symbol $\langle\ \rangle$ indicates time average over one period; G, the rate of increase of U due to stimulated emission, is given by

$$G = -\frac{1}{L}\int_{a-l/2}^{a+l/2}\langle \dot{P}(z,t)\,\mathcal{E}(z,t)\rangle\,dz\ , \qquad (52)$$

where the active medium is a sample of length l centered within the resonator at $z=a$; $\Omega = ck$ is the eigenfrequency of the empty resonator and, as before, ν is the laser frequency; Q is the quality factor of the resonator, taking into account losses due to transmission, diffraction, etc; and n_0, the index of refraction of the active medium (a real quantity), is a function of laser frequency and field intensity. Equations (50) have been written in a form which brings out their physical content. The first equation is the statement of energy balance within the resonator: The time rate of change of energy at any instant equals the net power increase due to induced emission and cavity loss. The second equation follows from frequency pulling considerations: The reflecting surfaces of the resonant cavity fix the laser wavelength, so as the refractive index varies, the oscillation frequency must change in order to satisfy the dispersion relation. Thus, the wavelength $\lambda = c/\Omega = v/\nu$, and Eq. (50b) follows from the definition $n_0 = c/v$.

It is convenient to define $P(t)$, the projection of induced polarization on the cavity mode:

$$P(t) = \frac{2}{L}\int_{a-l/2}^{a+l/2} P(z,t)\sin kz\,dz = \mathrm{Re}(\bar{\chi}\,\mathcal{E}_o e^{i\nu t})\ , \qquad (53)$$

where, from Eq. (48b),

$$\bar{\chi} = \frac{2}{L}\sum_{n\ \mathrm{odd}}\left(\chi_n^{+}\int_{a-\frac{1}{2}l}^{a+\frac{1}{2}l}\sin nkz\,\sin kz\,dz\right.$$

$$\left.+\,i\chi_n^{-}\int_{a-l/2}^{a+l/2}\cos nkz\,\sin kz\,dz\right)\ . \qquad (54)$$

Integrating over z, we find

$$\bar{\chi} = \frac{l}{L}\chi_1^{+} + \text{additional terms of the form}$$

$$\sum_{\text{odd } n}\frac{\lambda}{L}\frac{\chi_n^{\pm}}{n}\ . \qquad (55)$$

Because of the cavity boundary condition [Eq. (24)], the additional terms on the right-hand side vanish identically for $l=L$, the case where the sample fills the entire cavity, and in certain other cases. They will *always* be negligible so long as the y_n do not diverge for large n (since for an optical resonator, $\lambda/L \ll 1$). In any case, Eq. (53) may be used to transform Eqs. (50) into a form convenient for calculation. In the steady state, we find that

$$\mathrm{Im}\bar{\chi}(\nu, \mathcal{E}_o) = (4\pi Q)^{-1}\ , \qquad (56a)$$

$$\nu - \Omega = -2\pi\nu\,\mathrm{Re}\bar{\chi}(\nu, \mathcal{E}_o)\ . \qquad (56b)$$

In obtaining the latter expression we have made the approximation $n_0 = \sqrt{\epsilon} \cong 1 + 2\pi\,\mathrm{Re}\bar{\chi}$, with ϵ the capacitivity induced in the active medium by the laser field. To relate $\bar{\chi}$ to the Fourier coefficients, recall that as long as the y_n do not diverge for large n,

$$\bar{\chi} = \frac{l}{L}\chi_1^{+} = -2i\frac{\mu_o\bar{N}_o}{\mathcal{E}_o}\frac{l}{L}$$

$$\times\int_{-\infty}^{\infty} W(v)\left[\mathrm{Re}y_1 + i(\omega-\nu)\,\mathrm{Re}\left(\frac{y_1}{\gamma_{ab}+ik\nu}\right)\right]dv\ , \qquad (57)$$

so that

$$\mathrm{Re}\bar{\chi} = \frac{1}{2}\chi_{00}\frac{ku/\sqrt{\pi}}{\gamma_o^{\,s}}(\omega-\nu)\,\mathrm{Re}\int_{-\infty}^{\infty}\frac{W(v)y_1\,dv}{\gamma_{ab}+ikv} \qquad (58a)$$

and $$\mathrm{Im}\bar{\chi} = -\frac{1}{2}\chi_{00}\frac{ku/\sqrt{\pi}}{\gamma_0^{\,s}}\,\mathrm{Re}\int_{-\infty}^{\infty}W(v)y_1\,dv\ , \qquad (58b)$$

with $$\chi_{00} = \frac{\mu_o^{\,2}\bar{N}_o}{\hbar ku/\sqrt{\pi}}\,\frac{l}{L}\ , \qquad (58c)$$

the peak value of the imaginary part of the susceptibility of a Doppler-broadened gas with Doppler width ku (u is the most probable speed). Equations (56) and (58) implicitly determine the steady-state laser frequency and intensity in terms of the parameters of the laser medium and the resonator as soon as y_1 is determined.

5. GENERAL PROPERTIES OF FOURIER COEFFICIENTS (y_n)

It remains to solve Eqs. (43) and determine the explicit form of the Fourier coefficients. However, Eqs. (43) by themselves do not entirely specify the y_n's. In this connection, note that the nth equation ($n>0$) relates y_{n+1} to y_n and y_{n-1}. Thus, the first n equations of Eq. (43a), coupled with Eq. (43b), form a system of $n+1$ equations with $n+2$ unknowns so that only solutions for ratios involving pairs of y_n's, such as y_n/y_{n+1}, are possible. Accordingly, an additional piece of information is needed to explicitly obtain y_n. That piece of information is the asymptotic behavior of y_n/y_{n+1}, as $n\to\infty$.

To amplify this point, note that in the limit of large n (provided that $kv/\gamma_{ab}\neq 0$),

$$R_n \cong \tfrac{1}{2} inkv, \quad n \gg \frac{\gamma_{ab}}{k|v|}, \text{ and } \left|\frac{\omega-\nu}{kv}\right|, \tag{59}$$

so that Eq. (43a) may be written in the form

$$\left(\frac{inkv}{2\gamma_o \mathcal{S}}\right) y_n = y_{n+1} - y_{n-1}. \tag{60}$$

This difference equation has two types of solutions, characterized by the behavior of y_n for n large. The first is obtained by assuming

$$|y_{n-1}| > |y_{n+1}|, \quad \text{for } n \gg \frac{2\gamma_o \mathcal{S}}{k|v|}. \tag{61}$$

It follows that

$$\frac{y_{n-1}}{y_n} \cong -\frac{inkv}{2\gamma_o \mathcal{S}}, \tag{62}$$

$$\text{or} \quad y_n \propto (1/n!)(2i\gamma_o \mathcal{S}/kv)^n, \tag{63}$$

so that for sufficiently large values of n

$$y_n \to 0: \ B\text{-type solution.} \tag{64}$$

Because of their close connection with Bessel functions (see Appendix B), we shall refer to solutions of this kind as "B-type" solutions.

A second type of solution is obtained on the assumption that

$$|y_{n-1}| < |y_{n+1}|, \quad \text{for } n \gg 2\gamma_o \mathcal{S}/k|v|, \tag{65}$$

so that $$y_{n+1}/y_n \cong inkv/2\gamma_o \mathcal{S}, \tag{66}$$

or $$y_n \propto (n-1)!(ikv/2\gamma_o \mathcal{S})^n, \tag{67}$$

which implies that for n sufficiently large,

$$y_n \to \infty: \ N\text{-type solution}. \tag{68}$$

Because of their close connection with Neumann functions (see Appendix B), we shall refer to solutions of the latter type as "N-type" solutions.

A general solution to Eqs. (43) may be constructed from a linear combination of B-type and N-type solutions. However, in the problem at hand we reject the N-type solutions on several counts. In the first place, it is readily seen from the expressions for polarization and population inversion density, Eqs. (44) and (45), that condition (65), on which the latter-type solution is predicated, has the disturbing feature that successive *high-order* spatial harmonics in polarization and population inversion increase in magnitude, which goes against physical intuition. Secondly, Eq. (67) indicates that a *decrease* in field strength (which is proportional to $\mathcal{S}$) produces a corresponding *increase* in the magnitude of high-order spatial harmonics, contradicting results of weak-field perturbation theory. And finally, the N-type solutions lead, in principle, to the divergence of $\bar{\chi}$ [Eq. (55)], which enters into the expressions for laser power and frequency pulling [Eqs. (56)], since for n large the $n!$ dependence of y_n would dominate and the terms of the form $(\lambda/nL)\chi_n^{\pm}$ appearing in Eq. (60) would eventually diverge. Similar considerations also apply to the space-averaged population inversion density.

In contrast, the B-type solutions are well behaved in each of these respects. We therefore conclude that the solutions of interest are entirely of the B type, and that a necessary boundary condition supplementing Eqs. (43) is

$$\lim (y_{n+1}/y_n) = 0, \quad \text{as } n \to \infty. \tag{69}$$

In light of the above discussion, it is useful to rewrite the coupled difference equations in terms of the ratios

$$Z_n = -y_{n+1}/y_n. \tag{70}$$

Then Eqs. (43a) may be written in the form

$$Z_{n-1}=(R_n/\gamma_0 s+Z_n)^{-1}, \quad n=1,2,3,\ldots, \quad (71a)$$

subject to the boundary condition [Eq. (69)],

$$Z_n \to 0, \quad \text{as } n\to\infty . \quad (71b)$$

Equations (71) completely specify the Z_n's. Once Z_0 has been determined, y_0 may be obtained from Eq. (43b):

$$y_0=(1+4s\,\mathrm{Re}Z_0)^{-1} . \quad (72)$$

The other y_n's may then be sequentially generated from the definition

$$y_{n+1}=-Z_n y_n, \quad n=0,1,2,\ldots . \quad (73)$$

6. DETERMINATION OF Z_n AND THE FOURIER COEFFICIENTS

Solution for the General Case

Later in this section we shall obtain analytical expressions for the Z_n's in two important special cases, (a) $kv=0$, and (b) $\omega=\nu$ and $\gamma_a=\gamma_b$. We are not able to obtain an analytical solution to Eqs. (71) in the general case. However, we can write a general expression for Z_n as a continued fraction[3] which can be evaluated numerically to any desired accuracy. To this end, note that the successive application of Eq. (71a) for $n=1,2,3,\ldots$ leads to the continued fraction

$$Z_0=\cfrac{1}{R_1/\gamma_0 s+\cfrac{1}{R_2/\gamma_0 s+\cfrac{1}{R_3/\gamma_0 s+\cfrac{1}{\ddots+\cfrac{1}{R_{n'}/\gamma_0 s+Z_{n'}}}}}} , \quad (74)$$

from which successive Z_n's may be generated in sequence from Eq. (71a). The above expression does not necessarily converge to any one limit since, as we saw in Sec. 5, the difference equation from which it was derived has two possible types of limiting behavior. Accordingly, extreme care is required in numerically evaluating Eq. (74).

Specifically, we must compute Z_0, Eq. (74), in a manner consistent with the boundary condition

$$Z_n \to 0, \quad \text{as } n\to\infty . \quad (71b)$$

We are therefore encouraged to truncate the continued fraction after the first n' terms, which is equivalent to making the approximation that $Z_{n'} \equiv 0$. Denoting this approximate expression for Z_0 by $Z_0^{(n')}$ we compute $Z_0^{(n')}$, $Z_0^{(n'+1)}$, $Z_0^{(n'+2)}$, ..., continuing this process until we arrive at a value m such that the difference $|Z_0^{(m)}-Z_0^{(m-1)}|$ is less than a small predetermined value. We can then use $Z_0^{(m)}$ to obtain an approximate value for y_0 from Eq. (72), from which we can obtain values for y_1 and for all subsequent y_n's from Eqs. (71a) and (73).[22]

It is important to note that by setting $Z_m=0$ we also set $y_{m+1}=0$. It readily follows from Eq. (43a) that y_{m+2} is nonzero. Hence, automatically

$$|y_{m+2}|>|y_{m+1}| , \quad (75)$$

so that the computation of successively higher Fourier components unavoidably leads to N-type solutions, with y_n diverging for large n.[23] Such solutions are nonphysical, as discussed in Sec. 5. We conclude that the approximation $Z_0^{(m)}\simeq Z_0$ may be used with accuracy to compute only those y_n's for which n is somewhat less than m. In practice,

the calculation of high-order y_n's is also limited by the number of significant places retained in the computation of $Z_0^{(m)}$. For example, we have found that to obtain accurate values of y_n for $n \sim 30$, it is necessary to calculate $Z_0^{(m)}$ to 14 or 15 places of accuracy (using double-precision arithmetic).[22] On the other hand, for large values of n,

$$\left(n \gg \left|\frac{\omega - \nu}{kv}\right|, \frac{\gamma_{ab}}{k|v|}, \frac{2\gamma_o \$}{k|v|}\right),$$

y_n may be calculated directly from Eq. (63). This procedure provides a consistent way to calculate all desired Fourier coefficients. In fact, we have used Eq. (63) to check our y_n's computed from $Z_0(m)$ for large n such that $m \gg n$ and find excellent agreement.

Exact Solution for No Atomic Motion

For the special case in which atomic motion may be ignored, i.e., for a fully homogeneously broadened line ($\gamma_{ab}/k \gg$ rms atomic velocity), exact expressions for the Fourier coefficients may readily be obtained.[24] We shall outline the method, which illustrates the nature of the two types of solutions referred to in Sec. 5 and the behavior of the corresponding high-order Fourier coefficients.

To begin, note that in the limit $kv/\gamma_{ab} \to 0$, the R_n's [Eqs. (42)] reduce to

$$R_{n'} = \frac{\gamma_{ab}^2 + (\omega - \nu)^2}{2\gamma_{ab}}, \quad n' \text{ odd}, \tag{76a}$$

$$R_{n''} = \frac{\gamma_a \gamma_b}{2\gamma_{ab}} = \frac{1}{2}\gamma_o, \quad n'' \text{ even}, \tag{76b}$$

so that $R_{n'}$ and $R_{n''}$ become independent of n' and n'', respectively. Defining

$$R^2 = R_{n'} R_{n''} = \frac{\gamma_o}{4\gamma_{ab}}\left[\gamma_{ab}^2 + (\omega - \nu)^2\right], \tag{77}$$

one finds from Eq. (43a) that

$$R^2 y_n = (\gamma_o \$)^2 (y_{n+2} - 2y_n + y_{n-2}), \quad n > 1, \tag{78}$$

a second-order difference equation with constant coefficients. Equation (78) may be solved by assuming a solution of the form

$$y_{n'} = r^{n'-1} y_1, \tag{79a}$$

$$y_{n''} = r^{n''} y_0. \tag{79b}$$

Inserting either of these expressions into Eq. (78), one finds a quadratic equation in r^2 with solutions

$$r_\pm^2 = 1 + \tfrac{1}{2}(R/\gamma_o \$)^2 \{1 \pm [1 + (2\gamma_o \$/R)^2]^{1/2}\}. \tag{80}$$

It is evident from this expression that

$$0 \leq r_-^2 \leq 1, \tag{81a}$$

while $$r_+^2 \geq 1 \tag{81b}$$

for all values of R and $\$$. Inserting Eq. (79b) into Eq. (43a) for $n = 1$, and combining the resulting expression with Eq. (43b), we find

$$y_0^\pm = [1 + 2(\gamma_o \$/R)^2 (1 - r_\pm^2)]^{-1} = \mp [1 + (2\gamma_o \$/R)^2]^{-1/2}, \tag{82a}$$

and $$y_1^\pm = \frac{-1}{4\$}\{1 \pm [1 + (2\gamma_o \$/R)^2]^{-1/2}\}. \tag{82b}$$

As discussed in Sec. 5, we require that $y_n \to 0$ for large n. Hence, from Eqs. (81) and (79), only the r_- solution is physically acceptable. To verify this choice, note that in Eq. (82a) only the y_0^- solution is consistent with Eqs. (40b) and (42b), which require $y_0 = +1$ in the absence of fields ($\$ \to 0$). Also, in this limit $y_1^- \to 0$, while y_1^+ diverges. Accordingly, the y_0^+ and y_1^+ solutions (and therefore r_+) are unphysical. It can be seen from Appendix C that they y_n^- solutions are closely related to the B-type solutions of Sec. 5, whereas the y_n^+ solutions are closely related to the N-type solutions.[25]

Exact Solutions for $\omega = \nu$ and $\gamma a = \gamma b$ for Arbitrary Field Strength

In this important special case[26] we have been able to find exact analytical expressions for the Fourier coefficients.[27] Defining $\gamma_a = \gamma_b \equiv \gamma$, Eqs. (42) for the R_n's reduce to

$$R_n = \tfrac{1}{2}(\gamma + inkv), \quad n = 0, 1, 2, \ldots. \tag{83}$$

Accordingly, our difference equation (43a) reduces to

$$y_{n+1} - y_{n-1} = (1/2\$)[1 + i(kv/\gamma)n] y_n, \quad n = 1, 2, 3, \ldots. \tag{84}$$

It is shown in Appendix B that the above equation may be readily transformed into the well-known

recursion formula for cylindrical ("Bessel") functions.[28] Its general solution is

$$y_n = i^n[\mathfrak{B}(kv/\gamma, \mathcal{S})J_{n-i(\gamma/kv)}(4\gamma\mathcal{S}/kv) + \mathfrak{N}(kv/\gamma, \mathcal{S})J_{-n+i(\gamma/kv)}(4\gamma\mathcal{S}/kv)], \quad n = 0, 1, 2, \ldots , \tag{85}$$

where B and $\mathfrak{N}$ are independent of n. The standard notation $J_\nu(z)$ is used here to designate the Bessel function of (complex) order ν and argument z. We shall suppress the argument of the J's when convenient.

It is well known[28] that for large values of n

$$J_{n-i\epsilon} \sim 1/n! \ , \tag{86a}$$

and

$$J_{-n+i\epsilon} \sim (n-1)! \tag{86b}$$

so that, in accordance with the discussion of Sec. 5, we immediately conclude that $\mathfrak{N} = 0$ in Eq. (85). The value of $\mathfrak{B}$ may be obtained by inserting the surviving term of Eq. (85) into Eq. (72):

$$\mathfrak{B}J_{-i\gamma/kv} = \left[1 + 4\mathcal{S}\,\mathrm{Im}\left(\frac{J_{1-i\gamma/kv}}{J_{-i\gamma/kv}}\right)\right]^{-1} . \tag{87}$$

Thus, the desired solution is

$$y_n(kv/\gamma, \mathcal{S}) = i^n(J_{n-i\gamma/kv}/J_{-i\gamma/kv}) \times \left[1 + 4\mathcal{S}\,\mathrm{Im}\left(\frac{J_{1-i\gamma/kv}}{J_{-i\gamma/kv}}\right)\right]^{-1} , \text{ for all } n. \tag{88}$$

We can test this expression in the limiting case of $kv/\gamma \to 0$. It is shown in Appendix C that

$$\lim_{kv/\gamma \to 0} -i\left(\frac{J_{1-i\gamma/kv}(4\gamma\mathcal{S}/kv)}{J_{-i\gamma/kv}(4\gamma\mathcal{S}/kv)}\right) = (-1/4\mathcal{S})\{1 - [1 + (4\mathcal{S})^2]^{1/2}\} . \tag{89}$$

Thus, Eq. (88) for $n = 0$ has the limiting form

$$y_0 = [1 + (4\mathcal{S})^2]^{-1/2}, \quad kv/\gamma \to 0 , \tag{90}$$

in agreement with the physically acceptable solution y_0^- of Eq. (82a) in the limit $\gamma_a = \gamma_b$ and $\omega = \nu$.[29]

We have computed the Fourier coefficients from Eq. (88), evaluating the complex Bessel functions on the MIT 360 computer using double precision arithmetic. These quantities have also been computed from the continued fraction expression [Eq. (74)] using the procedure described at the beginning of this section. The advantage of dealing with Bessel functions is that they may be expanded in a series which converges absolutely and uniformly for all finite values of order and argument[28]:

$$J_\nu(z) = \sum_{m=0}^{\infty} \frac{(-)^m(\tfrac{1}{2}z)^{\nu+2m}}{m!\,\Gamma(\nu+m+1)} . \tag{91}$$

The results provide a convenient check on our method of evaluating the continued fraction.

Our calculations employ a simple iterative technique for calculating the Bessel series. We stop the iteration when the absolute value of the $m+1$th term is less than 10^{-6} of the preceding term. Consequently, the results are valid to at least five significant places for $kv/\gamma > 0.1$. For small values of kv/γ, the series becomes unwieldy. However, the $kv/\gamma = 0$ term may be calculated directly from Eqs. (79), (80), and (82). The excellent fit of these points with the rest of the curve demonstrates the reliability of our computer calculations.

Rate Equation Approach

The single-mode laser problem has also been treated[7] by the rate equation approximation, in which population fluctuations are neglected. These results may easily be derived from our coupled difference equations by neglecting all Fourier coefficients other than y_0 and y_1. Then Eqs. (43) reduce to

$$y_0 = 4\mathcal{S}\,\mathrm{Re}\,y_1 + 1 , \tag{92a}$$

$$y_1 = -\gamma_0\mathcal{S}\left(\frac{1}{\mathfrak{L}_1^+} + \frac{1}{\mathfrak{L}_1^{-*}}\right) y_0 , \tag{92b}$$

which immediately yields

$$y_0 = \left[1 + 4\gamma_c\gamma_{ab}\mathcal{S}^2\left(\frac{1}{|\mathfrak{L}_1^+|^2} + \frac{1}{|\mathfrak{L}_1^-|^2}\right)\right]^{-1} . \tag{93}$$

7. RESULTS AND DISCUSSION

The Fourier coefficients have been numerically evaluated by computer, as explained above. For the case $\omega = \nu$, $\gamma_a = \gamma_b$, $kv \neq 0$ we have computed the y_n's from the complex Bessel function solutions, Eq. (88). For the general case the y_n's have been approximated from the continued fraction expressions [Eqs. (72)–(74)] using the procedure explained in Sec. 6. For the case $kv = 0$, we have evaluated the y_n's directly from Eqs. (79), (80), and (82). The results are displayed in the following figures. For convenience, we define

$$I = 8\frac{\gamma_a\gamma_b}{\gamma_{ab}^2}\, s^2 = \tfrac{1}{2}\left(\frac{\mu_o \mathcal{E}_o}{\hbar}\right)^2 \frac{1}{\gamma_a\gamma_b} \qquad (94)$$

as a measure of intensity within the laser resonator.

Figure 2 plots the Fourier coefficients for the case $\gamma_a = \gamma_b$, $\omega = \nu$, obtained from the Bessel function expressions. These curves are essentially identical (agreement better than 0.01%) to curves computed using the continued fraction approximation, verifying the validity of such an approximation when appropriate precautions are taken (see Sec. 6). In each case, we find that the y_n's rapidly approach zero as n increases.

Stenholm and Lamb[3] have computed similar Fourier coefficients from a continued fraction expression[30] equivalent to our Z_0, Eq. (74). To compare their results with ours, we have plotted similar curves with the parameters of Ref. 3 ($\gamma_a/\gamma_{ab} = 0.6$, $I = 3.2$, $\omega = \nu$) using our continued fraction approximation. The comparisons are made in Fig. 3. For small n the two curves are in agreement in each case. However, for large n our curves approach zero $\sim 1/n!$ in accord with the discussions of Secs. 5 and 6, whereas those of Ref. 3 rapidly diverge. Evidently, the divergences result from attempts to evaluate y_n from a continued fraction terminated after m terms where $m < n$ (see discussion of Sec. 6).

The properties of the amplifying medium are completely specified by the velocity averaged susceptibility $\bar{\chi}(\nu-\omega, I)$ of Eq. (58). The imaginary part of $\bar{\chi}$, which is proportional to the single-pass gain induced by the standing wave field, is given by[31]

$$\mathrm{Im}\bar{\chi} = -\chi_{00}\frac{ku/\sqrt{\pi}}{\gamma_o s}\,\mathrm{Re}\int_0^\infty W(v) y_1\, dv\ . \qquad (95)$$

The real part of $\bar{\chi}$, which is closely related to the index of refraction as influenced by the standing-wave field, is given by[31]

$$\mathrm{Re}\bar{\chi} = \chi_{00}\frac{ku/\sqrt{\pi}}{\gamma_o s}(\omega-\nu)\,\mathrm{Re}\int_0^\infty \frac{W(v) y_1\, dv}{\gamma_{ab} + ikv}\ . \qquad (96)$$

Typical curves of $\mathrm{Im}\bar{\chi}(\nu-\omega)$ and $\mathrm{Re}\bar{\chi}(\nu-\omega)$ are plotted in Figs. 4 and 5, respectively, for various values of I. These have been generated by substituting the computed values of y_1 into Eqs. (95) and (96) and then performing the indicated integrations. We have taken $W(v)$ to be a Maxwellian velocity distribution of width $ku = 25\gamma_{ab}$:

$$W(v) = \exp[-(v/u)^2]/u\sqrt{\pi}, \quad ku = 25\gamma_{ab}\ . \qquad (97)$$

The integrations are performed by dividing the integrands into trapezoids of width $kv/\gamma_{ab} = 0.15$ and summing their areas from zero to a maximum value of kv/γ_{ab} such that the area of the last trapezoid is less than 0.1% of the total integrated area. The curves of $\mathrm{Im}\bar{\chi}$ versus $(\nu-\omega)/\gamma_{ab}$, Fig. 4, generally follow the corresponding Doppler-broadened gain profiles, except that for $|\omega-\nu| \lesssim \gamma_{ab}(1+I/2)^{1/2}$ a resonant decrease occurs. This effect, well known from third-order theory,[1,2] results from the fact that the coupling between the standing-wave field and the atomic system increases sharply as the frequency of the field is tuned to the center of the atomic resonance. The curves of $\mathrm{Re}\bar{\chi}$ versus $(\nu-\omega)/\gamma_{ab}$, Fig. 5, exhibit a broad background response which is an odd function of the detuning parameter $(\nu-\omega)/\gamma_{ab}$, characteristic of dispersion curves, with additional structure manifesting itself for small values of detuning. As with the $\mathrm{Im}\bar{\chi}$ curves, the latter structure results from the nonlinear coupling between the standing-wave field and the Doppler-broadened resonance, as described

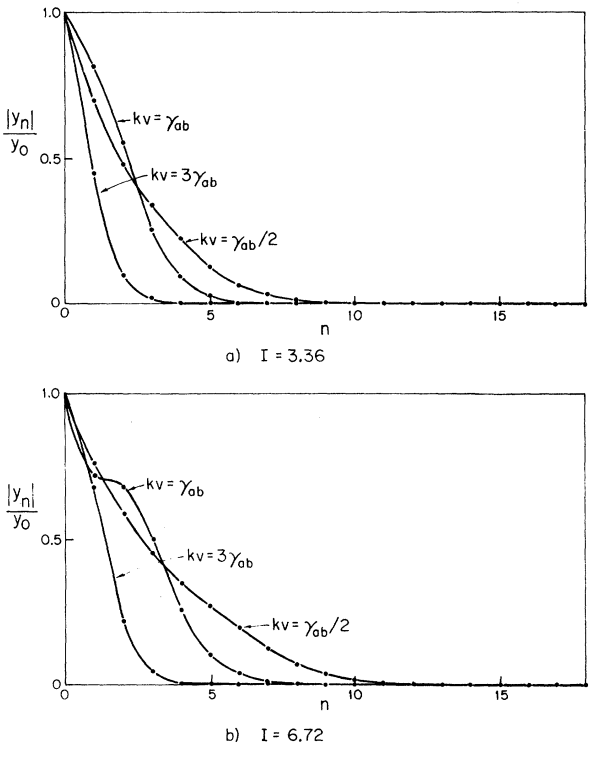

FIG. 2. Magnitudes of Fourier coefficients of induced polarization and population inversion density y_n. The coefficients, normalized such that $y_0 = 1$, are plotted for the case $\nu = \omega$ and $\gamma_a = \gamma_b$ for $kv/\gamma_{ab} = 0.5$, 1, and 3 for two intensities (a) $I = 3.36$ and (b) $I = 6.72$. The points, obtained from the Bessel-function expressions [Eq. (88)], are in complete agreement with values obtained using the continued fraction expression [Eq. (74)]. Note that with increasing n the y_n's rapidly decrease to 0.

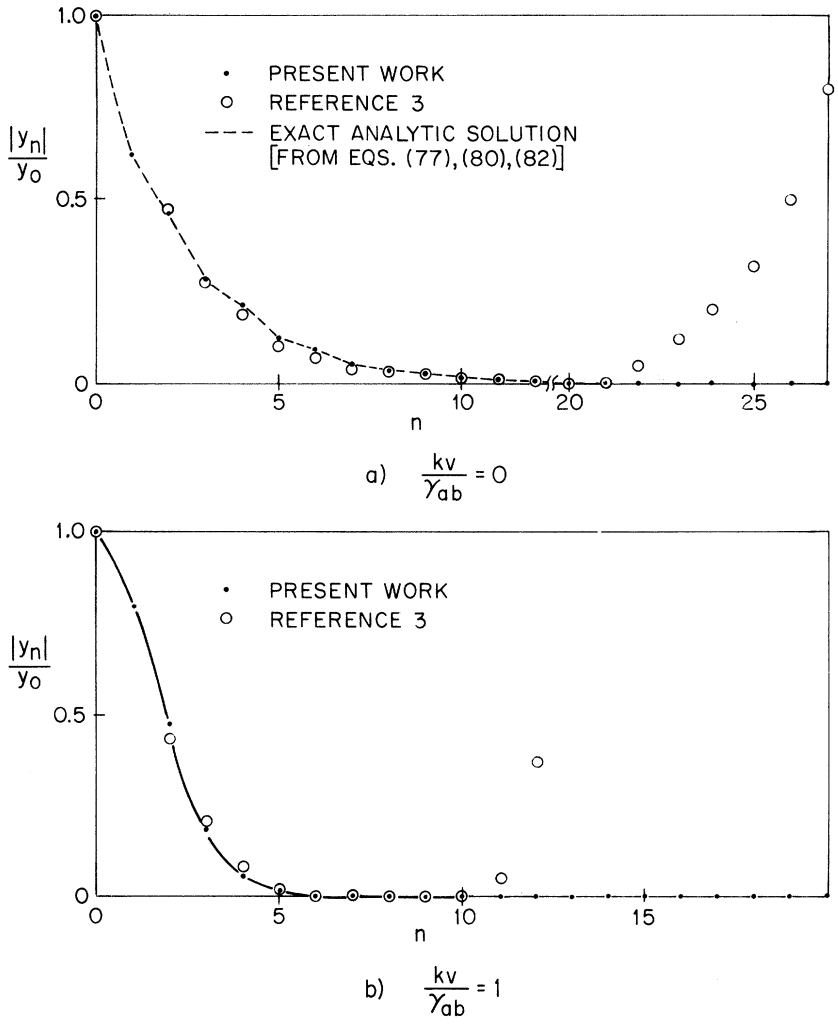

FIG. 3. Magnitudes of the (normalized) Fourier coefficients for the case $\nu = \omega$, $\gamma_a/\gamma_{ab} = 0.6$, and $I = 3.2$ for 2 values of v: (a) $kv/\gamma_{ab} = 0$ and (b) $kv/\gamma_{ab} = 1$. The points (black dots), generated from the continued fraction expression by the method of Sec. 6, are compared with the algebraic expression for $kv/\gamma_{ab} = 0$ (dashed curve) and the results of Stenholm and Lamb (Ref. 3) (open circles). Note that for large n the points of Ref. 3 diverge, whereas our computed values approach 0.

above. These results are compared to similar expressions obtained from the rate equation approximation,[7] Eqs. (92a) and (93) (dashed curves in Figs. 4 and 5). As can be seen, the rate equation approximation is not reliable at large values of field strength for small values of detuning.

The laser output power and frequency are implicitly determined by the fixed parameters, cavity loss ($\propto Q^{-1}$), cavity detuning frequency ($\Omega - \omega$) and the linear gain of the amplifying medium ($\propto \chi_{00}$) through Eq. (56):

$$\mathrm{Im}\bar{\chi}(\nu - \omega, I) = (4\pi Q)^{-1} , \tag{98a}$$

$$\Omega - \omega = (\nu - \omega) + 2\pi\nu \mathrm{Re}\bar{\chi}(\nu - \omega, I) . \tag{98b}$$

We can replot the data of Fig. 4 in the form of $\mathrm{Im}\bar{\chi}$ versus I for various values of $(\omega - \nu)/\gamma_{ab}$. Equation (98a) indicates that for fixed loss the laser intensity is determined as a function of $\nu - \omega$ along lines of constant $\mathrm{Im}\bar{\chi}$. Thus, we may readily plot curves of I versus $\nu - \omega$ by drawing lines of constant loss and reading off I as a function of $\nu - \omega$ at the points of intersection. The results are shown in Fig. 6, which indicates a central tuning dip (Lamb-dip) for intense fields which does not qualitatively differ from the third-order result,[2] except that the dip deepens and broadens with increasing ratio of gain to loss. The above procedure was first used by Stenholm and Lamb[3] who studied curves of I as a function of $\nu - \omega$ in detail. We have recalculated their curves to verify them and generally find close agreement.[32]

The dispersion relation [Eq. (98b)] introduces "pushing" and "pulling" effects on the actual laser frequency, so that an experimental measurement of intensity versus cavity detuning $(\Omega - \omega)$ would lead to results somewhat different from the curves of Fig. 6. A complete analysis would require solving the coupled equations (98). However, the results of Fig. 5 suggest that for large fields $\mathrm{Re}\bar{\chi}$ does not greatly vary as a function of I. Accord-

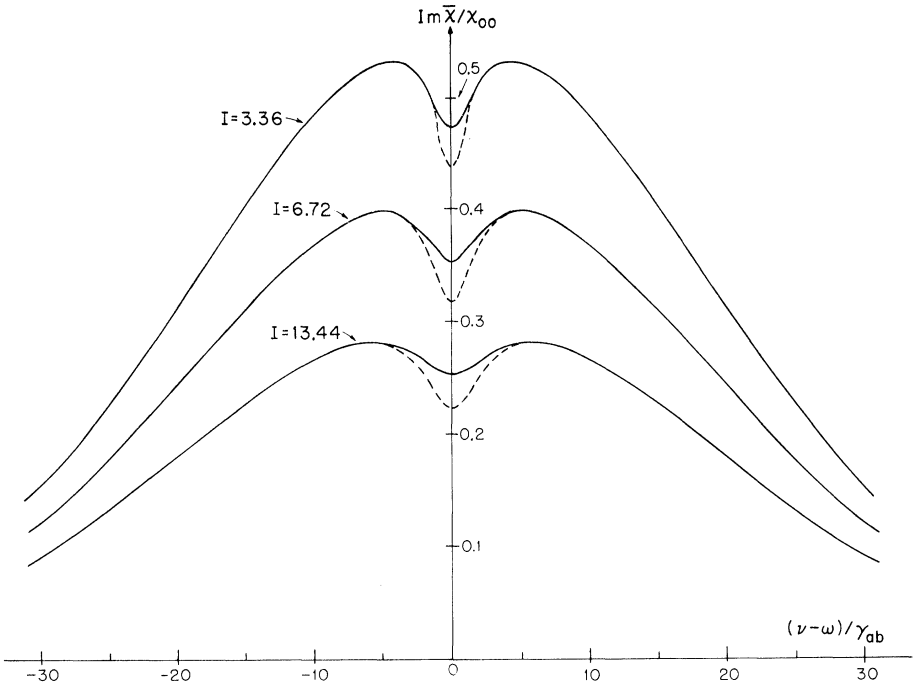

FIG. 4. Curves for Im$\bar{\chi}$ versus $\nu-\omega$ for various values of I. Im$\bar{\chi}$ is given in units of χ_{00} [Eq. (58c)]. Figures 4–6 are plotted for the case $\gamma_a=\gamma_b$ and $ku/\gamma_{ab}=25$. Note that Im$\bar{\chi}$ is proportional to the single-pass gain of the amplifying medium subjected to a standing-wave field. The corresponding results predicted by the rate-equation approximation [Eqs. (92) and (93)] are shown as dashed lines.

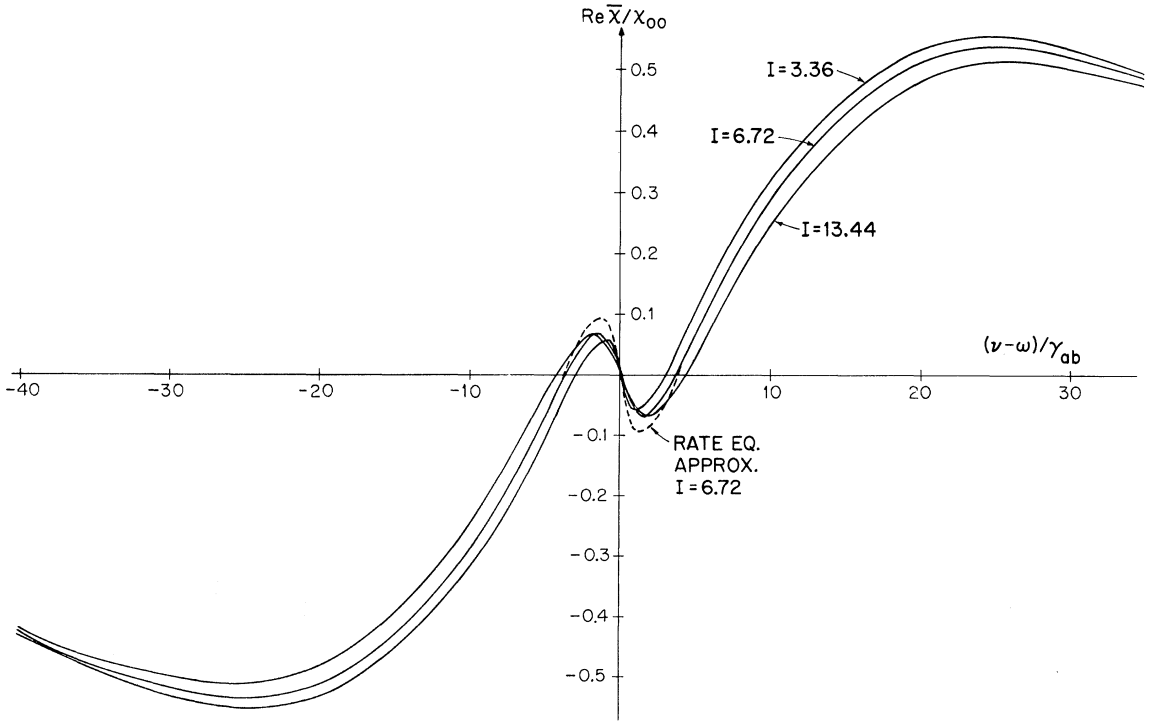

FIG. 5. Curves for Re$\bar{\chi}$ versus $\nu-\omega$ for various values of I. Re$\bar{\chi}$ is given in units of χ_{00} [Eq. (58c)]. Note that Re$\bar{\chi}$ is a measure of the dispersion of the amplifying medium as influenced by the intense standing-wave field.

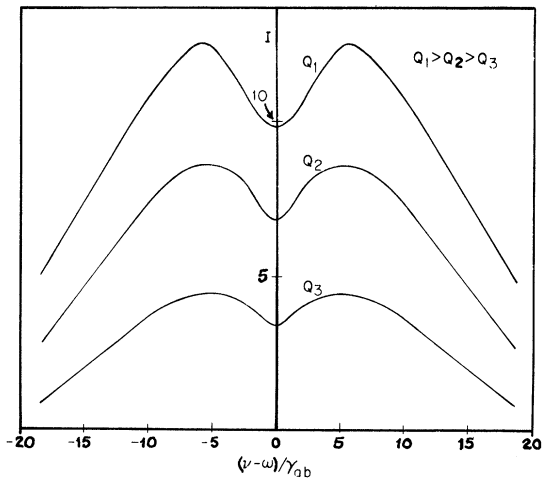

FIG. 6. Curves of I versus $(\nu-\omega)/\gamma_{ab}$ obtained from points of intersection with line of constant $\mathrm{Im}\bar{\chi}=(4\pi Q)^{-1}$. Curves are drawn for 3 values of Q: $Q_1=0.27/\chi_{00}$, $Q_2=0.22/\chi_{00}$, and $Q_3=0.17/\chi_{00}$.

ingly, for intense fields the dispersion relation is more or less independent of field strength so that, as a first approximation, the coupled equations (98) may be treated independently.

In addition to the laser output curves, we have plotted the spatially averaged population inversion density,[33]

$$\bar{N}(v)=\frac{1}{L}\int_{a-\frac{1}{2}l}^{a+\frac{1}{2}l} N(v,z,t)\,dz$$

$$=\bar{N}_0(l/L)W(v)y_0(v)\ , \qquad (99)$$

as a function of kv/γ_{ab} for various values of the detuning parameter, $(\omega-\nu)/\gamma_{ab}$. These curves, computed from the continued fraction approximation of Sec. 6, are shown in Fig. 7. For $|\omega-\nu| \gtrsim \gamma_{ab}(1+2I)^{1/2}$, two narrow resonant decreases occur symmetrically located about the center of the broad velocity distribution. These depletions result from the fact that to an ensemble of atoms moving with axial velocity v the standing-wave field appears as two oppositely directed travelling-wave fields Doppler shifted to frequencies $\nu\pm kv$. Accordingly, for large values of detuning two narrow atomic velocity bands centered at $v=\pm(\omega-\nu)/k$ will resonantly couple to the standing-wave field producing the observed depletions, the stronger the interaction the broader and deeper the depletions. As $|\omega-\nu|\to 0$, the two regions of depletion begin to overlap, and at $\omega=\nu$ a single depletion is observed at the center of the velocity distribution. For moderate values of field strength ($I \gtrsim 1$), we find that additional structure develops about the center of the depletion (Fig. 8). This structure is

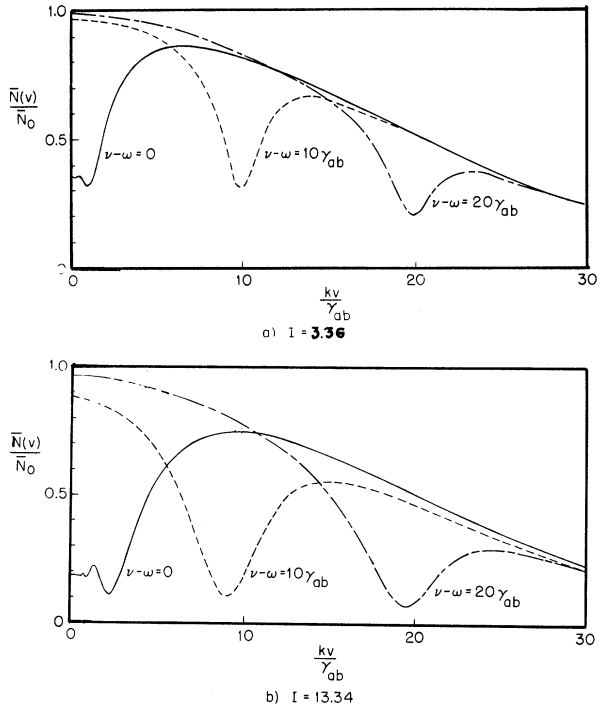

FIG. 7. Space-averaged population inversion density $\bar{N}(v)$ as a function of kv for various values of detuning. The curves are normalized to the excitation density $\bar{N}_0$ Curves are plotted for $(\nu-\omega)/\gamma_{ab}=0$, 10, and 20 for two values of relative intensity: (a) $I=3.36$ and (b) $I=13.44$. In the figure, $\gamma_a=\gamma_b$ and $ku/\gamma_{ab}=25$.

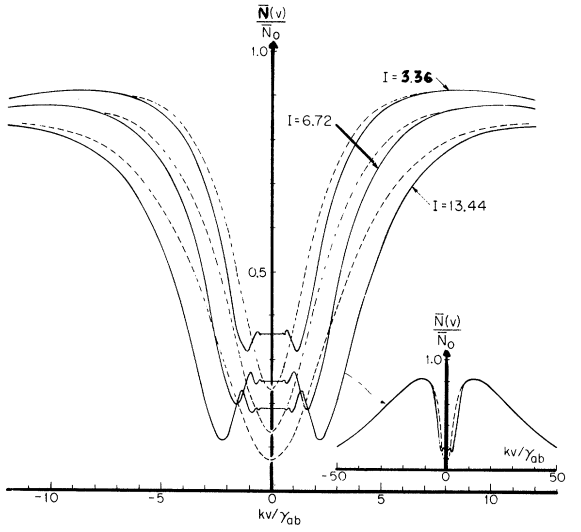

FIG. 8. Space-averaged population inversion density $\bar{N}(v)$ normalized to the excitation density $\bar{N}_0$. The curves are plotted for $\omega=\nu$, $\gamma_a=\gamma_b$, and $ku/\gamma_{ab}=40$ for relative intensities $I=3.36$, 6.72, and 13.44. For comparison, the corresponding curves obtained from the rate equation approximation are also plotted (dotted lines).

remarkable in that the strongest decreases occur not for fixed atoms but for slowly moving ones ($|v| \sim \gamma_{ab}/k$), hence atoms which, by virtue of the Doppler effect, are somewhat detuned from resonance. This structure is not observed in calculations based on third-order[2] and fifth-order[11] perturbation calculations, nor in rate equation treatments.[7] To verify these findings, we have recomputed the $\omega = \nu$ curve from the exact Bessel-function expression [Eq. (88a)]. We find excellent agreement, thus confirming the existence of the new structure as noted by Stenholm and Lamb.[3]

To understand the nature of this new effect, we find it useful to examine the normalized population inversion density [Eq. (45)],

$$N(v,z,t)/N_o = y_0 + 2\,\mathrm{Re} \sum_{\text{even } n>0} y_n e^{inkz}, \quad (100)$$

as a function of kz for various values of kv/γ_{ab}. These quantities have been plotted in Fig. 9 for the case $\omega = \nu, \gamma_a = \gamma_b$ for two values of $I > 1$. They have been computed from our Bessel-function expressions for the y_n's [Eq. (88a)], terminating the series at the mth term such that $|y_m|/|y_0| < 10^{-6}$. For very-low-velocity atomic ensembles ($|v| \ll \gamma_{ab}/k$), the spatial variations impressed upon the inversion density are similar in form to the $v = 0$ expression, $N(0,z,t)$ of Ref. 25. For high velocity ensembles, the spatial variations are of negligible size. In the interesting intermediate region, $|v| \sim \gamma_{ab}/k$, the spatial variations, though sizable, no longer follow the $v = 0$ result. At certain values of kz the inversion density drops below the minimum of the $v = 0$ curve, and for sufficiently intense fields it can actually become *negative*, which may reduce the corresponding space-average below the space average of the $v = 0$ curve.

This dramatic effect is inherently linked with the standing wave nature of the laser field. To analyze the situation, recall that in the rest frame of an atomic ensemble moving with given velocity [rest frame coordinates $\{z', t'\}$], the applied standing wave field appears as a pair of oppositely directed travelling wave components of frequencies $\nu_\pm = \nu \mp k\nu$. Since these components are intense, they can couple nonlinearly to one another provided that their frequency separation is of the order of or less than the atomic relaxation rate: $|\nu_+ - \nu_-| = 2k|v| \lesssim \gamma_a + \gamma_b$. If the latter condition is satisfied, the field components couple parametrically in the laser medium to produce population sidebands which vary at even harmonics of kvt' and polarization sidebands which vary at odd harmonics of kvt', as viewed in the atomic rest frame. As is shown in Appendix A, the normalized population inversion density in the atomic rest frame is given by

$$N(v,z',t')/N_o = y_0 + 2\,\mathrm{Re} \sum_{\text{even } n>0} y_n(v) e^{inkvt'} e^{inkz'}, \quad (101)$$

where the familiar quantity y_n, previously obtained in the laboratory reference frame, may now be interpreted as the coefficient of the sideband component parametrically generated at frequency nkv. We can conveniently illustrate Eq. (101) by means of a vector diagram, Fig. 10(a), which shows a cylinder of revolution bounded by the $|y_n|/y_0$ curve of Fig. 2 for $k|v|/\gamma_{ab} = \frac{1}{2}$. In each cross section of the cylinder, which represents the complex plane for the nth population sideband component, the vector $y_n \exp[ink(z' + vt')]$ is drawn. Note that the nth vector rotates counterclockwise at circular frequency nkv. The net in-

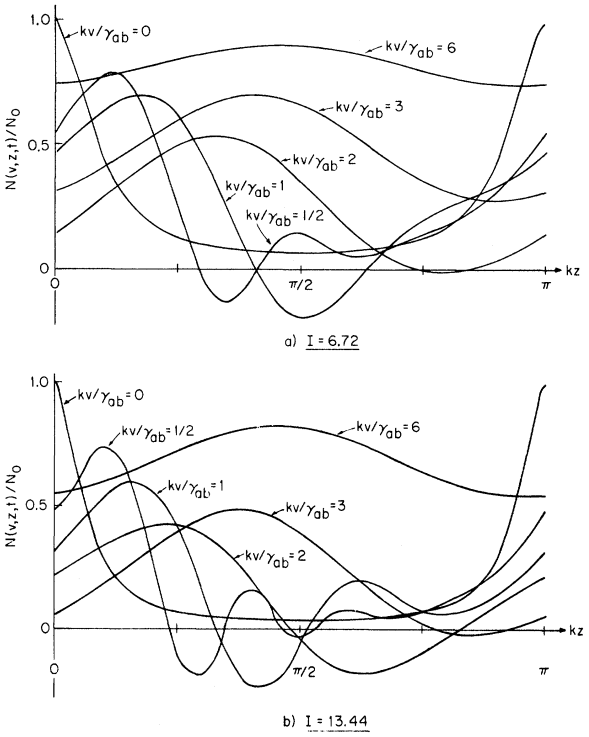

FIG. 9. Spatial variations of the inversion density, $N(v,z,t)$, for ensembles moving with different velocities. The curves are drawn for $\nu = \omega$ and $\gamma_a = \gamma_b$ for two values of I (a) 6.72 and (b) 13.44. In constructing Figs. 9 and 10, the velocity distribution has been assumed uniform over the range of kv's chosen. Note that for low values of kv/γ_{ab} the inversion density actually reverses in sign and becomes negative at certain values of kz. For weaker fields the inversion density may not change sign but can still fall below the minimum inversion for the $v = 0$ case. (See Fig. 8 of Ref. 3.)

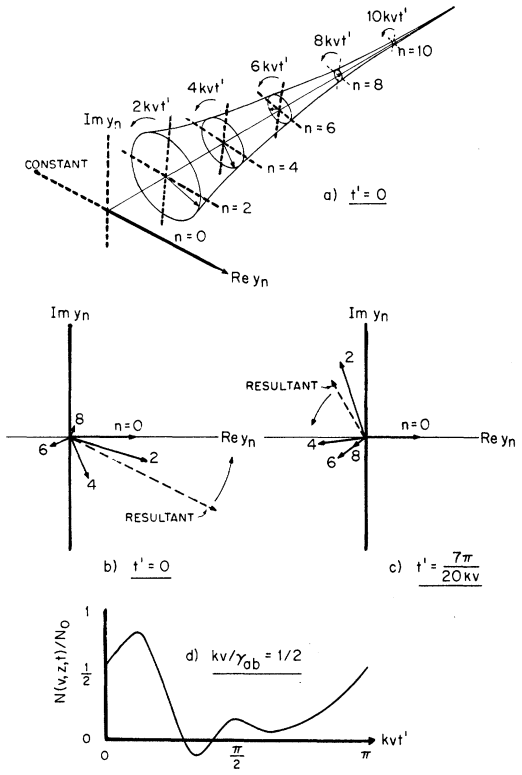

FIG. 10. Analysis of the spatial variations in inversion density in the ensemble rest frame. The moving atoms see the intense standing-wave field as a pair of travelling-wave components at frequencies $\nu_{\pm}=\nu\mp kv$. The intense fields mix parametrically in the medium, producing population sidebands at multiples of $2kv$. The figure has been constructed for the case $\gamma_a=\gamma_b$ and $I=6.72$ at moving frame coordinate $z'=0$ at different values of t': (a) The nth population sideband may be viewed as a vector y_n, n even, rotating in the complex plane at frequency $2kvt'$. The net inversion density at time t' is the projection onto the real axis of the sum of all of the vectors. The conical envelope is a cylinder of revolution bounded by the $|y_n|/y_0$ curve of Fig. 2(b) for $kv/\gamma_{ab}=0.5$. (b) Front view of Fig. 9(a) at $t'=0$. (c) Same at $t'=7\pi/20kv$. The resultant vector lies in the second quadrant, indicating that the inversion density has reversed in sign. (d) Time variation of the inversion density, as viewed at $z'=0$ in the moving frame.

version density is given by the sum of all of the vectors projected onto the real axis. Due to the fact that the vectors rotate at even harmonics of kv, the resulting sum will vary periodically in time. At most values of t', the resulting projection is positive. Figures 10(b) and 10(c), viewed normal to the cylinder axis, show the vector diagrams at $t'=0$ and $t'=7\pi/20k|v|$, respectively, for $z'=0$. Note that the resulting projection in Fig. 10(c) is negative, indicating a negative value of inversion density at that time. Thus, viewed in the ensemble rest frame, the inversion density appears to vary periodically in time, becoming negative at some points in the cycle [Fig. 10(d)].

This oscillatory behavior may be viewed as a coherent ringing of the population inversion density. An atomic ensemble at velocity v and position z' passing through the standing-wave field experiences an intense amplitude modulated field of the form

$$\mathcal{E}_0 \sin(kvt'+kz')\cos\nu[t'+(v/c^2)z'] \ . \qquad (102)$$

The way in which the ensemble responds depends strongly on the ratio of the modulation frequency kv to the rate of relaxation $\sim\gamma_{ab}$. An ensemble which experiences very slow modulation ($k|v| \ll\gamma_{ab}$) can closely follow changes in the envelope of the applied field; consequently, it responds at every instant as if subjected to a field of constant intensity. In contrast, an ensemble experiencing rapid modulation ($k|v|\gg\gamma_{ab}$) cannot follow at all, so that the inversion density ceases to respond. However, when the modulation rate is comparable to the relaxation rate ($k|v|\sim\gamma_{ab}$) the inversion density responds sizably but cannot instantaneously readjust to the changing amplitude of the envelope of the applied field. The inversion density continually overshoots its corresponding steady-state value, producing a phase shift and ringing [Fig. 10(d)]. The detailed behavior of the response varies with field intensity.

The reversal in sign of the inversion density may also be understood qualitatively in analogy with short pulse effects. In this view, the applied field, a sinusoidal envelope of "pulses" of alternating sign on carrier frequency ν, acts on the atomic ensemble as would an infinite train of pulses separated in time by $\pi/k|v|$. For an ensemble which experiences roughly one pulse per relaxation period ($|v|\sim\gamma_{ab}/k$), the possibility arises that for appropriate field strengths the pulse can flip the population of the levels during a portion of the cycle in much the same manner as would a π pulse [Fig. 10(d)]. Note, however, that an ensemble of high velocity ($|v|\gg\gamma_{ab}/k$) experiences several pulses, alternating in sign, within a relaxation period so that on the average the effect of the pulses tends to cancel.

To summarize, we have seen that in the rest frame of an atomic velocity ensemble, the inversion density will undergo periodic time variations which may become negative at some portion of the cycle. Using the transformation $z=z'+vt'$, it is easy to see that the temporal variations in the rest frame appear as spatial variations in the laboratory frame, thus explaining the features of Fig. 9. [Note that the $k|v|/\gamma_{ab}=\frac{1}{2}$ curve of Fig. 9(a) is

identical to Fig. 10(d).]

Having explored the velocity and spatial dependence of the net inversion density $N(v,z,t)$, we are able to understand the origin of the new structure in the velocity distribution of the spatially averaged inversion density $\bar{N}(v)$. In considering this average, note that for $|v| \sim \gamma_{ab}/k$ the very small and/or negative values of $N(v,z,t)$ at some points in space can have the effect of reducing the averaged values there below those for $v \approx 0$, accounting for the fine structure of $\bar{N}(v)$, Fig. 8. [Each point on an $\bar{N}(v)$ curve (Fig. 8) is essentially the area under the corresponding $N(v,z,t)$ curve of Fig. 9.]

Similar fine structure does not appear in the power output curves, Fig. 6, essentially determined by the single-pass gain [Eq. (52)], which is proportional to $\int_{-\infty}^{\infty} \mathrm{Re} y_1(v) W(v) dv$. The integrand of the latter quantity is plotted in Fig. 11 for several small values of $(\omega - \nu)/\gamma_{ab}$. This curve is closely related to $\bar{N}(v)$ [see Eq. (43b)] and exhibits a similar fine structure. However, the fine structure does not manifest itself in the power output curves since the area under $\mathrm{Re} y_1(v) W(v)$ does not change appreciably for slight detuning from the atomic center frequency.

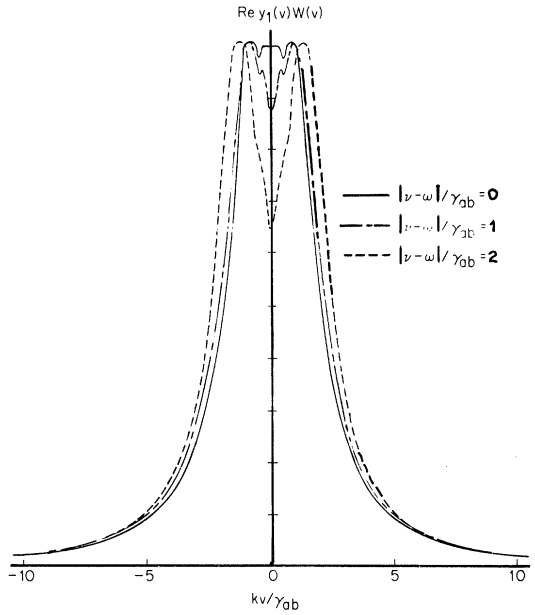

FIG. 11. Velocity dependence of the space-averaged out-of-phase component of the induced polarization $\mathrm{Re} y_1(v) W(v)$, for small values of detuning. The figure is drawn for the case $I = 6.72$, $\gamma_a = \gamma_b$, and $ku/\gamma_{ab} = 25$. The single-pass gain for a particular value of detuning $(\nu - \omega)/\gamma_{ab}$ is proportional to the area under the corresponding curve. Since the areas in the figure are all about the same, the fine structure exhibited in the velocity distribution curves does not manifest itself in the tuning dip of the single-pass gain curves (Fig. 4).

8. CONCLUDING REMARKS

We are also studying the influence of the population fine structure on the gain profile of a second transition optically coupled to either of the levels of the laser transition.[6] In important special cases analytical solutions have been obtained for a laser field of arbitrary intensity. The results will shortly be submitted for publication.

The results of this paper may also be applied in studying the "inverted" Lamb-dip,[34] which is observed by introducing a resonant absorber into the laser cavity.[35] In this case an additional saturable loss must be included in the energy-balance relation, Eq. (56a), which becomes

$$\mathrm{Im}\bar{\chi}_{\mathrm{amp}}(\nu, I) + \mathrm{Im}\bar{\chi}_{\mathrm{abs}}(\nu, I) = 1/4\pi Q \ , \qquad (103)$$

where $\bar{\chi}_{\mathrm{amp}}$ and $\bar{\chi}_{\mathrm{abs}}$ are the velocity averaged susceptibilities of the amplifier and absorber, respectively, as given by Eq. (57).

ACKNOWLEDGMENTS

The authors thank Professor Steve Orzag for useful discussions, Professor Abraham Szöke for helpful kibitzing, Peter Birk, Mike Frankston, and Julius Goldhar for enthusiastic assistance with the computer work, and Miss Gloria Nickerson and Miss Jennifer Lewis for typing the manuscript. One of us (MSF) thanks Professor John Waugh for an interesting discussion on microwave resonance theory. Most importantly, every phase of this work has benefited from the discussions and encouragement of Professor Ali Javan.

APPENDIX A: ENSEMBLE-AVERAGED DENSITY MATRIX IN THE REST FRAME OF THE ATOMIC ENSEMBLE

In this Appendix, we show how one can utilize the ensemble-averaged equations of motion in the rest frame of an ensemble moving with velocity v to obtain a solution equivalent to the laboratory frame solution derived in the text. Consider an atomic ensemble comprised of all those atoms in the medium travelling with axial velocity components in a narrow interval between v and $v + dv$. In the laboratory system [coordinates $\{z,t\}$], the atoms experience a standing-wave field,

$$\mathcal{E}(z,t) = \mathcal{E}_o \sin kz \cos \nu t \ , \qquad (A1)$$

which may be decomposed into two oppositely directed travelling-wave components at frequency ν:

$$\mathcal{E}(z,t)=\tfrac{1}{2}\mathcal{E}_o[\sin(\nu t+kz)-\sin(\nu t-kz)]\ . \quad \text{(A2)}$$

Viewed in a coordinate system in which the atoms are at rest, [coordinates $\{z',t'\}$], the field components, Doppler shifted in frequency to $\nu\pm$, are given by

$$\mathcal{E}(z',t')=\tfrac{1}{2}\mathcal{E}_o[\sin(\nu_- t'+k_- z')-\sin(\nu_+ t'+k_+ z')]$$

$$=\frac{1}{4i}\mathcal{E}_o[\{A_-(z')e^{i\nu_- t}-A_+(z')e^{i\nu_+ t}]-\text{c.c.}\}, \quad \text{(A3)}$$

where $\nu_\pm=\nu\mp kv$, (A4a)

$$k_\pm=\nu_\pm/c\ , \quad \text{(A4b)}$$

and $A_\pm(z')=e^{\mp ik_\pm z'}$. (A4c)

In the moving frame the total and partial time derivatives are equal,

$$\frac{d}{dt}=\frac{\partial}{\partial t'}+v\frac{\partial}{\partial z'}\rightarrow\frac{\partial}{\partial t'}\ , \quad \text{(A5)}$$

so that spatial dependence is transformed out – spatial variations only enter in through the phase factors of the field amplitudes. Accordingly, the ensemble-averaged density matrix equations of motion [Eq. (22)] become

$$\frac{\partial}{\partial t'}\rho(v,z',t')=-\frac{i}{\hbar}[H(z',t'),\rho(v,z',t')]$$

$$-\tfrac{1}{2}\{\Gamma,[\rho(v,z',t')-\rho^0(v,z',t')]\}\ , \quad \text{(A6)}$$

so that in the moving frame the problem reduces to the interaction of two applied fields at frequencies $\nu_\pm$ with a stationary atomic ensemble. The frequencies combine in the nonlinear medium to produce polarization and population sidebands. Close inspection of Eq. (A6) indicates that we may conveniently expand the elements of ρ in the following Fourier series:

$$\rho_{ab}(v,z',t')$$

$$=\sum_{m=0}^{\infty}[\Pi^+_{2m+1}A^*_+(A_-A^*_+)^m e^{-i\nu_+ t'}e^{im(\nu_- -\nu_+)t'}$$

$$+\Pi^-_{2m+1}A^*_-(A_+A^*_-)^m e^{-i\nu_- t'}e^{im(\nu_+ -\nu_-)t'}]\ , \quad \text{(A7)}$$

$$\rho_{aa}(v,z',t')$$

$$=n_a+\sum_{m=0}^{\infty}[a_{2m}(A_-A^*_+)^m e^{im(\nu_- -\nu_+)t'}+\text{c.c.}], \quad \text{(A8a)}$$

$$\rho_{bb}(v,z',t')$$

$$=n_b+\sum_{m=0}^{\infty}[b_{2m}(A_-A^*_+)^m e^{im(\nu_- -\nu_+)t'}+\text{c.c.}]. \quad \text{(A8b)}$$

Note that these expansions have been written in a form in which the phase factors $A_\pm$ have been taken out of the Fourier coefficients $\Pi_n^\pm$, a_n, and b_n. We may obtain relationships among the Fourier coefficients by inserting the diagonal and off-diagonal elements of ρ into the equation of motion [Eq. (A6)] and equating coefficients of like temporal harmonics. This procedure leads to a set of coupled difference equations identical in form to the set obtained in the laboratory frame, Eqs. (29) and (31). Once having obtained expressions for the Fourier coefficients, we may transform $\rho(\nu,z',t')$ back into the laboratory frame. This transformation is facilitated by noting that the arguments of the sine functions of $\mathcal{E}(z',t')$, Eq. (A3), are phases which are invarient under coordinate transformations

$$\nu_\pm t'\mp k_\pm z'\rightleftharpoons\nu t\mp kz\ . \quad \text{(A9)}$$

Also note that the Fourier coefficients, being independent of z' and t', are unaffected by the transformation. Accordingly, one finds that in the lab frame the components of $\rho(v,z,t)$ are

$$\rho_{ab}(v,z,t)=e^{-ivt}\sum_{m=0}^{\infty}(\Pi^+_{2m+1}e^{i(2m+1)kz}$$

$$+\Pi^-_{2m+1}e^{-i(2m+1)kz})\ , \quad \text{(A10)}$$

$$\rho_{aa}(v,z,t)=n_a+\sum_{m=0}^{\infty}(a_{2m}e^{2imkz}+\text{c.c.})\ , \quad \text{(A11a)}$$

$$\rho_{bb}(v,z,t)=n_b+\sum_{m=0}^{\infty}(b_{2m}e^{2imkz}+\text{c.c.})\ , \quad \text{(A11b)}$$

so that the results are identical to those obtained in the laboratory frame.[36]

APPENDIX B: SOLUTION TO THE LINEAR DIFFERENCE EQS. (84) AND (60)

Consider the homogeneous linear difference equation (84), which may be written in the form

$$y_{n+1} - y_{n-1} = (a + ibn) y_n \ , \tag{B1}$$

where $a = 1/2s$ (B2a)

and $b = kv/2\gamma s$. (B2b)

Making the transformation[37]

$$y_n = i^n C_\nu \ , \tag{B3a}$$

$$\nu = n - ia/b \ , \tag{B3b}$$

and defining $z = 2/b$, (B4)

one obtains

$$C_{\nu+1}(z) + C_{\nu-1}(z) = (2\nu/z) C_\nu(z) \ , \tag{B5}$$

the well-known recursion formula for cylindrical functions.[28] The general solution is a combination of two linearly independent cylindrical functions, which for ν not an integer may be written

$$C_\nu(z) = \mathfrak{B} J_\nu(z) + \mathfrak{N} J_{-\nu}(z) \ , \tag{B6}$$

where $\mathfrak{B}$ and $\mathfrak{N}$ are constants and $J_\nu(z)$ denotes the Bessel function of order ν and argument z. Equation (85) follows directly from Eqs. (B3a) and (B6).

A similar difference equation which appears in Sec. 5, Eq. (60), is also of the form of Eq. (B1) with $a = 0$ and $b = kv/2\gamma_o s$. Accordingly, the two linearly independent types of solution are

$$y_n \propto i^n J_n(4\gamma_o s/kv) \ , \tag{B7a}$$

and $y_n \propto i^n N_n(4\gamma_o s/kv)$, (B7b)

where $N_n(z)$ is the Neumann function of order n and argument z. It is readily seen from the asymptotic expressions for Bessel functions of large order[28] that Eq. (B7a) corresponds to the B-type solutions [Eq. (63)], whereas, Eq. (B7b) corresponds to the N-type solutions [Eq. (67)].

APPENDIX C: LIMITING FORM OF ANALYTICAL SOLUTION (88); DERIVATION OF EQ. (89)

Consider the expression

$$Z_0^{\pm} = \frac{-iJ_{\mp(1 - i\gamma/kv)}(4\gamma s/kv)}{J_{\pm i\gamma/kv}(4\gamma s/kv)} \tag{C1}$$

[cf. Eq. (89)]. To obtain the limiting form of Eq. (C1) as $kv/\gamma \to 0$, we employ the asymptotic expansion for complex cylindrical functions of large order, first derived by Debye[38] using the method of steepest descent and later enlarged upon by Watson.[28] The relevant asymptotic expansions are

$$H_\nu^{(1)}(z) \to \frac{\exp[\nu(\tanh\Gamma - \Gamma) - \frac{1}{4}i\pi]}{[-(\frac{1}{2}i\nu\pi)\tanh\Gamma]^{1/2}} \tag{C2a}$$

and $H_\nu^{(2)}(z) \to \frac{\exp[-\nu(\tanh\Gamma - \Gamma) + \frac{1}{4}i\pi]}{[-(\frac{1}{2}i\nu\pi)\tanh\Gamma]^{1/2}}$, (C2b)

where $H_\nu^{(1)}(z)$ and $H_\nu^{(2)}(z)$ are Hankel functions

and $\cosh\Gamma = \nu/z$ (C3)

is subject to the restrictions

$$-\tfrac{1}{2}\pi < \arg(-i\sinh\Gamma) < \tfrac{1}{2}\pi \ , \tag{C4a}$$

$$|\arg z| < \tfrac{1}{2}\pi \ , \tag{C4b}$$

$$0 < \mathrm{Im}\,\Gamma < \tfrac{1}{2}\pi \ . \tag{C4c}$$

Defining $\cosh\Gamma_1 = \frac{1 - i\gamma/kv}{4\gamma s/kv}$, (C5a)

and $\cosh\Gamma_0 = \frac{-i\gamma/kv}{4\gamma s/kv}$, (C5b)

we find, consistent with the restrictions of Eqs. (C4), that to first order in kv/γ,

$$\tanh\Gamma_0 = -[1 + (4s)^2]^{1/2} \ , \tag{C6a}$$

$$\Gamma_0 = \ln\left(\frac{-1}{4s}\{1 - [1 + (4s)^2]^{1/2}\}\right) + \tfrac{1}{2}i\pi \ , \tag{C6b}$$

$$\tanh\Gamma_1 = \tanh\Gamma_0 \left(1 + \frac{kv}{i\gamma}\,\frac{(4s)^2}{1 + (4s)^2}\right) \ , \tag{C7a}$$

and $\Gamma_1 = \Gamma_0 + \frac{kv}{i\gamma}[1 + (4s)^2]^{-1/2}$. (C7b)

Consider now the limiting form of Z_0^-: Since[28]

$$J_\nu(z) = \tfrac{1}{2}[H_\nu^{(1)}(z) + H_\nu^{(2)}(z)] \ , \tag{C8}$$

we find that in the limit $kv/\gamma \to 0$,

$$\begin{aligned} Z_0^- = &-i\cosh[(1 - i\gamma/kv)(\tanh\Gamma_1 - \Gamma_1) - \tfrac{1}{4}i\pi] \\ &\times[-\tfrac{1}{2}(1 - i\gamma/kv)i\pi\tanh\Gamma_1]^{-1/2} \\ &\times\{\cosh[(-i\gamma/kv)(\tanh\Gamma_0 - \Gamma_0) - \tfrac{1}{4}i\pi] \\ &\times[-\tfrac{1}{2}(-i\gamma/kv)i\pi\tanh\Gamma_0]^{1/2}\}^{-1} \ . \end{aligned} \tag{C9}$$

Defining $\Lambda = -(i\gamma/kv)(\tanh\Gamma_0 - \Gamma_0)$, (C10)

and using Eqs. (C7), we find after some manipulation that

$$\lim Z_0^{-} = -i\frac{\cosh(\Lambda - \Gamma_0 - \frac{1}{4}i\pi)}{\cosh(\Lambda - \frac{1}{4}i\pi)}, \quad \text{as } kv/\gamma \to 0, \quad \text{(C11)}$$

where terms proportional to kv have now been dropped. Manipulating the hyperbolic functions to remove the $\frac{1}{4}\pi$ term, we obtain

$$\lim Z_0^{-} = -i\left[\cosh\Gamma_0 + \sinh\Gamma_0 \times\left(\frac{-\sinh\Lambda + i\cosh\Lambda}{\cosh\Lambda - i\sinh\Lambda}\right)\right], \text{ as } kv/\gamma \to 0. \quad \text{(C12)}$$

An examination of Eq. (C10) utilizing Eqs. (C6) reveals that as $kv/\gamma \to 0$, $\mathrm{Re}\Lambda \to -\infty$, so that

$$\lim Z_0^{-} = -i(\cosh\Gamma_0 + \sinh\Gamma_0) = -\frac{1}{4s}\{1 - [1 + (4s)^2]^{1/2}\}, \text{ as } kv/\gamma \to 0 \quad \text{(C13)}$$

as stated in Eq. (89) of the text.

The limiting expression for Z_0^{+} may be obtained in the same manner. If we note that[28]

$$J_{-\nu}(z) = \tfrac{1}{2}[e^{i\nu\pi}H_\nu^{(1)}(z) + e^{-i\nu\pi}H_\nu^{(2)}(z)], \quad \text{(C14)}$$

a similar calculation leads to

$$\lim Z_0^{+} = -\frac{1}{4s}\{1 + [1 + (4s)^2]^{1/2}\}, \quad \text{as } kv/\gamma \to 0. \quad \text{(C15)}$$

Combining this expression with Eq. (72), we obtain y_0^+ of Eq. (82a), which was rejected on physical grounds, an additional check that $\mathfrak{N} = 0$.

---

*Work supported by National Aeronautics and Space Administration.

[1]W. E. Lamb, Jr., in Quantum Electronics and Coherent Light, edited by C. H. Townes and P. A. Miles (Academic Press Inc., New York, 1964), p. 78.

[2]W. E. Lamb, Jr., Phys. Rev. 134, A1429 (1964).

[3]S. Stenholm and W. E. Lamb, Jr., Phys. Rev. 181, 618 (1969).

[4]P. H. Lee, P. B. Schoefer, and W. B. Barker, Appl. Phys. Letters 13, 373 (1968); M. S. Feld, A. Javan, and P. H. Lee, *ibid.* 13, 424 (1967); V. P. Chebotayev, I. M. Beterov, and V. N. Lisitsyn, IEEE J. Quantum Electronics, QE-4, 788 (1968).

[5]M. S. Feld, Ph. D. thesis, MIT, 1967 (unpublished).

[6]M. S. Feld and A. Javan, Phys. Rev. 177, 540 (1969).

[7]Treatments which ignore population pulsations in space or in time are called rate-equation approximations. See, for example, W. Culshaw, Phys. Rev. 164, 329 (1967); H. Greenstein, *ibid.* 175, 438 (1968); S. G. Rautian, Doctoral dissertation, Works Lebedev Inst., Acad. Sci., USSR, 43 (1968); see also Ref. 2, Sec. 18.

[8]See, for example, R. L. Fork and M. A. Pollack, Phys. Rev. 139, A1408 (1965); H. R. Schlossberg and A. Javan, *ibid.* 150, 267 (1966); R. L. Fork, A Dienes, and J. W. Kluver, IEEE J. Quantum Electronics QE-5, 607 (1969); M. Tsukakoshi and K. Shimoda, J. Phys. Soc. Japan 26, 758 (1969).

[9]M. Sargent, III, W. E. Lamb, Jr., and R. L. Fork, Phys. Rev. 164, 436 (1967).

[10]A. Dienes, Phys. Rev. 174, 400 (1968); 174, 414 (1968).

[11]For an extension of the treatment of Ref. 2 to 5th order see K. Uehara and K. Shimoda, J. Appl. Phys. Japan 4, 921 (1965).

[12]W. E. Lamb, Jr., and T. M. Sanders, Jr., Phys. Rev. 119, 1901 (1960).

[13]These considerations are amplified in Appendix A.

[14]We are grateful to Professor Haus for pointing out the convenience of working directly in the laser rest frame.

[15]Actually, atoms are produced in mixtures of stationary states with arbitrary phase factors. The random nature of these phase factors makes possible the assumption that atoms are produced in pure states.

[16]W. E. Lamb, Jr., and R. C. Retherford, Phys. Rev. 79, 549 (1950).

[17]A. Javan, Phys. Rev. 107, 1579 (1957).

[18]In evaluating the partial derivatives Leibnitz's formula may be used. For example,

$$\frac{\partial}{\partial t}\int_{-\infty}^{t} dt_o \rho[v, t; z - v(t - t_o), t_o, k] = \rho(v, t; z, t, k) + \int_{-\infty}^{t} dt_o \frac{\partial}{\partial t}\rho[v, t; z - v(t - t_o), t_o, k]. \quad (21)$$

[19]More precisely, we require

$$\frac{\partial n_{a,b}}{\partial z} \ll k n_{a,b} \quad \text{and} \quad \frac{\partial n_{a,b}}{\partial t} \ll \gamma_{ab} n_{a,b}$$

so that $\frac{\partial \Pi_n^{\pm}}{\partial z} \ll k\Pi_n^{\pm}$ and $\frac{\partial \Pi_n^{\pm}}{\partial t} \ll \gamma_{ab}\Pi_n^{\pm}$

and similar inequalities in a_n and b_n.

[20]See Eqs. (64) of Ref. 3.

[21]Note that Eq. (44) may be written in the equivalent form

$$P(v; z, t) = 2\mu_o N_o \mathrm{Im}[S\sin\nu t + C\cos\nu t],$$

with $S = \sum_{n \text{ odd}} y_n e^{inkz}$,

and $C=(\omega-\nu)\sum_{n\ \text{odd}}\frac{y_n e^{inkz}}{\gamma_{ab}+inkv}$.

[22]Alternate method: By independently computing Z_0, $Z_1,\ldots Z_{n-1}$ to a given accuracy from their continued fraction expressions, one can obtain more accurate values for y_n's of large n by means of the relation

$$y_n=(-)^n Z_{n-1}Z_{n-2}\cdots Z_0 y_0,$$

which easily follows from Eq. (73).

[23]This discussion assumes, as invariably occurs in practice, that the method of truncation outlined above results in a value of m sufficiently large to satisfy the inequality of Eq. (61).

[24]See Ref. 3, Appendix A.

[25]The well-known expressions for induced polarization and population inversion density follow directly from Eqs. (43), (44), (77), (79), (80), and (82) [for y_n^-]. After straightforward manipulation one obtains the familiar results

$$P(0,z,t)=\mathrm{Re}\left(\frac{\mu_o^2}{\hbar}\overline{N}_o \times\frac{[-(\omega-\nu)+i\gamma_{ab}]\mathcal{E}_0\sin kz e^{i\nu t}}{(\omega-\nu)^2+\gamma_{ab}^2+(4\mathcal{S})^2\gamma_o\gamma_{ab}\sin^2 kz}\right)$$

and $$N(0,z,t)=\overline{N}_o\frac{(\omega-\nu)^2+\gamma_{ab}^2}{(\omega-\nu)^2+\gamma_{ab}^2+(4\mathcal{S})^2\gamma_o\gamma_{ab}\sin^2 kz}.$$

[26]*Note added in manuscript*: Solutions in different forms have also been given by Rautian (Ref. 7) and by Stenholm, Phys. Rev. (to be published). Using an integral expression, Stenholm shows that for large I [see Eq. (94)], Eq. (56a) leads to $I\sim 4\pi Q\mu_o^2\overline{N}_o/\hbar\gamma$. This relationship is also obtainable from our Eq. (88) for $n=1$: From the usual asymptotic expansion for Bessel functions (Ref. 28, p. 199), it follows for $\mathcal{S}\gg 1$ and $\gamma\mathcal{S}/kv \gg 1$ that $4\mathcal{S}\ \mathrm{Im}\,[J_{1-i\gamma/kv}(4\gamma\mathcal{S}/kv)/J_{-i\gamma/kv}(4\gamma\mathcal{S}/kv)]\gg 1$, so that $\mathrm{Re}\,y_1\sim -1/4\mathcal{S}$. Stenholm's relationship then follows from Eqs. (56a) amd (58b).

[27]This exact solution also describes the polarization induced in a homogeneously broadened microwave resonance by an amplitude-modulated field of arbitrary strength of the form $\mathcal{E}(\phi,t)=\mathcal{E}_0\cos[\nu t+(\delta/\nu)\phi]\sin(\delta t+\phi)$, where $\delta=kv$ and $\phi=kz$ is an adjustable phase [see Eq. (102)]. This is the first time, to our knowledge, that such a solution has been obtained.

[28]G. N. Watson, A Treatise on the Theory of Bessel Functions, (Cambridge University Press, Cambridge, 1966), 2nd ed.

[29]Had we assumed, instead, that the boundary condition required $\mathcal{B}=0$, we would have found (Appendix C) that in the limit $kv/\gamma\to 0$,

$$y_o=-[1+(4\mathcal{S})^2]^{-1/2},$$

the nonphysical result of Eq. (82a).

[30]Reference 3, Eq. (68).

[31]In obtaining Eq. (95) from Eq. (58b), we have utilized the fact that $\mathrm{Re}\,y_1$ is even in v, as can be seen from Eqs. (72) and (73), noting that $\mathrm{Re}\,Z_0$ is even in v. Similarly, Eq. (98) follows from Eq. (58a) since $\mathrm{Im}\,Z_0$ is odd in v.

[32]This is true in spite of the diverging behavior of y_n found by Stenholm and Lamb (Ref. 3), since they neglect the additional terms of Eq. (55) on the assumption that the laser medium completely fills the resonator.

[33]This expression ignores the negligible contributions arising from higher-order Fourier coefficients as in the discussion following Eq. (55).

[34]P. H. Lee and M. L. Skolnick, Appl. Phys. Letters 10, 303 (1967); S. N. Bagaev, Yu. D. Kolomnikov, V. N. Lisitsyn, and V. P. Chebotaev, J. Quantum Electronics QE-4, 868 (1968); R. L. Barger and J. L. Hall, Phys. Rev. Letters 22, 4 (1969); G. R. Hanes and K. M. Baird, Metrologia 5, 32 (1969); V. M. Tatarenkov, A. N. Titov, and A. V. Uspenskii, Proceedings of the All-Union Scientific Research Institute for Physical-Technical and Radio-Technical Measurements (VNIIFTRI) Report No. 28, 1969 (unpublished).

[35]This is the configuration used in obtaining intense single moding in Ref. 4.

[36]*Note added in manuscript*. Expansions similar to Eqs. (A7) and (A8) have been recently employed by Shimoda to obtain a perturbation expansion in I for the standing-wave polarization: K. Shimoda, Proceedings of Sixth Chania International Meeting on Short Laser Pulses and Coherent Interactions, Chania, Crete (to be published).

[37]E. W. Barnes, Messenger Math. 34, 52 (1905).

[38]P. Debye, München. Sitzber. 40 (1910).